

EXPERIMENTAL STUDY OF POST-INSTALLED ANCHORS UNDER COMBINED SHEAR AND TENSION LOADING

**Mark K. Johnson
H. S. Lew**

**U.S. DEPARTMENT OF COMMERCE
National Institute of Standards
and Technology
National Engineering Laboratory
Center for Building Technology
Structures Division
Gaithersburg, MD 20899**

**U.S. DEPARTMENT OF COMMERCE
Robert A. Mosbacher, Secretary
Lee Mercer, Deputy Under Secretary
for Technology
NATIONAL INSTITUTE OF STANDARDS
AND TECHNOLOGY
John W. Lyons, Director**

NIST

EXPERIMENTAL STUDY OF POST-INSTALLED ANCHORS UNDER COMBINED SHEAR AND TENSION LOADING

**Mark K. Johnson
H. S. Lew**

**U.S. DEPARTMENT OF COMMERCE
National Institute of Standards
and Technology
National Engineering Laboratory
Center for Building Technology
Structures Division
Gaithersburg, MD 20899**

March 1990



**U.S. DEPARTMENT OF COMMERCE
Robert A. Mosbacher, Secretary
Lee Mercer, Deputy Under Secretary
for Technology
NATIONAL INSTITUTE OF STANDARDS
AND TECHNOLOGY
John W. Lyons, Director**

ABSTRACT

The behavior of post-installed anchors subjected to static combined shear and tension loads was studied experimentally. Twenty-four 1 in. diameter wedge-type expansion anchors were tested in uncracked concrete. Anchors were not preloaded and were located sufficiently far from the edge of the concrete specimens. Test variables included the angle of inclination of applied load (measured with respect to a horizontal plane), anchor embedment depth, and concrete compressive strength. Shear failures occurred for specimens tested at load angles between 0 and 60° and tension failures were observed for specimens tested at load angles between 60 and 90°. There were two types of shear failures: steel fracture near the bottom of the anchor at the tapered section for anchors with shallow embedment depths and steel fracture along the shank for more deeply-embedded anchors. Two types of tension failures occurred: steel tensile failure at the threads and cone-shaped tensile failure of the concrete. For specimens failing in shear, anchor capacity depended mainly on embedment depth. A limiting capacity was reached at an embedment depth of approximately 6 in. when steel failure controlled. Anchor deformation was influenced by both load angle and embedment depth.

Keywords: anchors; combined loading; concrete; embedment depth; expansion anchors; post-installed anchors; shear; tension.

TABLE OF CONTENTS

LIST OF TABLES	vii
LIST OF FIGURES	ix
1.0 INTRODUCTION	1
1.1 General	1
1.2 Objectives and Scope	2
2.0 EXPERIMENTAL PROGRAM	3
2.1 Introduction	3
2.2 Specimen Fabrication	3
2.2.1 Specimen Details	3
2.2.2 Fabrication Details	4
2.2.3 Material Properties	5
2.3 Specimen Testing	6
2.3.1 Test Set-Up	6
2.3.2 Instrumentation	7
2.3.3 Test Procedure	8
2.4 Summary	9
3.0 RESULTS OF EXPERIMENTAL PROGRAM	19
3.1 Ultimate Loads and Modes of Failure	19
3.2 Behavior of Anchor Specimens	20
3.2.1 Specimens With $\phi = 0^\circ$	20
3.2.2 Specimen With $\phi = 22.5^\circ$	23
3.2.3 Specimens With $\phi = 45^\circ$	24
3.2.4 Specimens With $\phi = 60^\circ$	28
3.2.5 Specimens With $\phi = 70$ to 90°	31
3.2.6 Effect of Load Angle	34
3.3 Summary of Test Results	38
4.0 DISCUSSION AND CONCLUSIONS	65
4.1 Discussion of Test Results	65

4.1.1	Deformation Behavior of Anchors	65
4.1.2	Ultimate Behavior of Anchors	67
4.2	Conclusions	71
REFERENCES	73

LIST OF TABLES

Table	Page
2.1 Details of Testing Program	10
3.1 Test Results of Experimental Program	41
3.2 Depth of Spalled Concrete for Specimens With $\phi = 45^\circ$	42
3.3 Effect of Load Angle on Ultimate Behavior	43
3.4 Concrete Spalling Loads	44

LIST OF FIGURES

Figure	Page
2.1 Anchor Bolt Details	11
2.2 Concrete Slab Details	12
2.3 Fabricated Anchor Specimen	13
2.4 Stress-Strain Curve for Tensile Coupon of Wedge-Type Expansion Anchor	13
2.5 Stress-Strain Curves for Concrete Cylinders	14
2.6 Test Set-Up	15
2.7 Details of Test Set-Up	16
2.8 Instrumentation of Anchor Specimen	17
3.1 Applied Loading Condition	45
3.2 Types of Shear Failures	45
3.3 Types of Tension Failures	46
3.4 Load-Displacement Curves for Specimens With $\phi = 0^\circ$ and $l_d = 4.0$ and 5.25 in.	47
3.5 Anchor Fracture at Reduced Section of Specimen 27	48
3.6 Anchor Fracture at Shank of Specimen 33	49
3.7 Load-Displacement Curves for Specimens With $\phi = 0^\circ$ and $f_c \approx 4500$ and 6000 psi	50
3.8 Load-Displacement Curve for Specimen With $\phi = 22.5^\circ$	51
3.9 Horizontal Components of Load-Displacement Curves for Specimens With $\phi = 45^\circ$ and $l_d = 5.25$ in.	52
3.10 Anchor Capacity Versus Embedment Depth for Specimens With $\phi = 45^\circ$	52
3.11 Load-Displacement Curves for Specimens With $\phi = 45^\circ$ and $f_c \approx 6000$ psi	53
3.12 Horizontal Components of Load-Displacement Curves for Specimens With $\phi = 60^\circ$ and $l_d = 4.0$ and 5.25 in.	54
3.13 Anchor Tensile Failure at Threads of Specimen 19	55
3.14 Anchor Capacity Versus Embedment Depth for Specimens With $\phi = 60^\circ$	55

3.15	Load-Displacement Curves for Specimens With $\phi = 60^\circ$ and $f_c \approx 4500$ psi	56
3.16	Broken Failure Cone of Specimen 23	57
3.17	Failure Cone of Specimen 4	58
3.18	Vertical Components of Load-Displacement Curves for Specimens With $\phi = 70$ to 90°	59
3.19	Anchor Capacity Versus Load Angle for Specimens With $l_d = 4.0$ and 5.25 in.	60
3.20	Anchor Capacity Versus Embedment Depth for Specimens With $\phi = 45$ and 60°	61
3.21	Anchor Capacity Versus Embedment Depth for Specimens With $\phi = 0$ to 90°	62
3.22	Load-Displacement Curves for Specimens With $l_d = 4.0$ in. and $f_c \approx 4500$ psi	63
3.23	Load-Displacement Curves for Specimens With $l_d = 5.25$ in. and $f_c \approx 4500$ psi	64
4.1	Interaction Diagrams for Wedge-Type Anchors	72

1.0 INTRODUCTION

1.1 General

Anchors may be installed into hardened concrete to provide a mechanical connection to the concrete element. These anchors, termed post-installed anchors, are used in many applications, including the attachment of structural elements to each other and the attachment of equipment to floors, ceilings, and walls.

One important use of post-installed anchors is in strengthening existing building structures. In this application, anchors are used to connect strengthening elements to the existing structure. Strengthening may be required to satisfy new building code requirements, improve the capacity of a building for additional anticipated loads, or restore the capacity of a damaged building.

The use of post-installed anchors in strengthening existing buildings is currently being investigated at the National Institute of Standards and Technology. In this investigation, the effectiveness of various strengthening techniques in improving the lateral load-carrying capacity and ductility of reinforced concrete frames is being evaluated. A literature review of strengthening methodologies[1] found that the behavior of strengthened frames depends not only on the properties of the frame and strengthening element but also on the interaction between the two elements provided by the anchors. Therefore, determining the behavior of strengthened frames requires an understanding of the behavior of anchors subjected to the loading conditions at a wall/frame interface. Specifically, knowledge of the response of anchors to combined shear and tension loading is needed.

A literature review of post-installed anchors[2] revealed that testing of such anchors in combined shear and tension loading has been reported[3,4,5] and that interaction diagrams for anchor capacity have been presented[5,6,7]. However, detailed knowledge of the behavior of

post-installed anchors under combined loading and the effects of such variables as anchor embedment depth and relative magnitude of applied shear and tension loads on that behavior are lacking.

1.2 Objectives and Scope

The aim of this experimental program is to gain an understanding of the strength and deformation behavior of post-installed anchors under combined shear and tension loading and the factors that affect this behavior. The results of this study are to be used to help assess the behavior of strengthened frame systems.

This experimental program is limited to the study of wedge-type expansion anchors, a common type of torque-controlled expansion anchor. In addition, only single anchors embedded in uncracked concrete with a large edge distance are considered.

2.0 EXPERIMENTAL PROGRAM

2.1 Introduction

The experimental program involved the testing of 24 anchor specimens under static combined shear and tension loading. Specimens consisted of 1 in. diameter post-installed wedge-type expansion anchors embedded in holes drilled into uncracked concrete slabs. The anchors were located far from the edge of the concrete slab and were not preloaded.

Table 2.1 presents details of the testing program. Three variables were investigated: (1) the angle of inclination of the applied load, (2) the compressive strength of the concrete slab, and (3) the embedment depth of the anchor. The angle of inclination of applied load, ϕ , measured with respect to a horizontal plane, varied from 0° (pure shear) to 90° (pure tension) and had values of 0, 22.5, 45, 60, 70, 80, and 90° . The concrete strength, f_c , varied from 4350 to 6350 psi and specimens were grouped into two broad strength ranges: 4500 psi and 6000 psi. The anchor embedment depth, l_d , ranged from 3.0 to 6.25 in. Except for Specimen 4, all specimens satisfied the manufacturer's minimum embedment depth requirement of 3-1/2 in.

2.2 Specimen Fabrication

2.2.1 Specimen Details

The wedge-type anchors used in this study, shown in Figure 2.1(a), were composed of AISI 12L14 carbon steel. They were made up of a smooth shank with threads at one end and a tapered section at the other end. At the tapered section, there was a two-piece wedge mechanism with protrusions which provided a means of engaging the anchor to the wall of the drilled hole. A reduction in cross sectional area occurred at the junction of the shank and the tapered end (at section a-a in Figure 2.1(a)). The shank diameter was 1.00 in., whereas the diameter of

section a-a was 0.81 in. The diameter of the taper increased from 0.81 in. at section a-a to 1.00 in. at the end of the anchor. Section a-a will hereafter be referred to as the reduced section.

The concrete slabs into which the anchors were installed, shown in Figure 2.2, were 48 in. long, 30 in. wide, and 16 in. deep. They were cast on five different occasions. In the first four casts, longitudinal reinforcement consisting of two No. 6 Grade 60 deformed bars was provided at the top of the slab and 1 in. diameter ducts were cast into the bottom of the slab for lifting. In the last cast, no reinforcement was provided and ducts were placed at the mid-depth of the slab so that anchors could be tested on both the top and bottom faces of the slab. In all the slabs, vertical 2-1/2 in. diameter ducts were located at the corners to permit the slab to be attached to supports during testing. Anchors were located in drilled holes at the center of the face of the slab. The distance to the edge of the slab was equal to one half of the slab width, or 15 in., and was sufficiently large so as to not have any effect on anchor behavior. In addition, longitudinal reinforcement was located far enough away from the anchor so that it did not influence anchor behavior.

2.2.2 Fabrication Details

Fabrication of anchor specimens involved the casting of concrete slabs and the subsequent installation of anchors. To cast the slabs, formwork was first built. Five forms were constructed so that specimens were cast in sets of five. Next, the forms were prepared for casting by inserting horizontal and vertical ducts and, for the slabs which were nominally reinforced, by adding steel reinforcement.

Specimens were cast using concrete supplied by a ready-mix concrete manufacturing company. One of the company's standard concrete mixtures was used. The concrete consisted of Type I Cement (611 lb/yd³), 1 in. maximum size crushed aggregate, sand, water, and a water reducer. In the five casts, the concrete slump ranged from 3 to 4-1/2 in. and the

air content ranged from 2 to 2-1/2%. During casting of the slabs, 4 x 8 in. concrete cylinders were also cast. Both the slabs and cylinders were stripped after three days and cured together.

After the slabs had cured for at least 28 days, the anchors were installed. A hole was drilled using a 1 in. diameter rotary percussion masonry drill bit to a depth of 6 to 7 inches. After drilling, dust was blown out of the hole and the anchor was hammered into it to the desired depth. Washers were then placed around the anchor and a nut was screwed onto the anchor and torqued to 300 ft-lb as specified by the manufacturer (see Figure 2.1(b)). Torquing the nut caused the body of the anchor to lift approximately 1/2 in. out of the hole, forcing the fixed wedge mechanism to bear against the wall of the hole to provide mechanical anchorage. The definition of embedment depth used in this study was the distance from the concrete surface to the bottom of the wedge mechanism (see Figure 2.1(b)). After seating the wedge mechanism in the hole, the anchor nut was untorqued. Thus the preload induced in the anchor during installation was removed prior to testing. Figure 2.3 shows a completely fabricated anchor specimen.

2.2.3 Material Properties

Material properties of the wedge-type expansion anchors were determined by tension tests. Two coupon specimens were fabricated from wedge-type anchors. Each specimen was instrumented with an extensometer and tested in uniaxial tension to failure. The resulting stress-strain curves for the two specimens were almost identical. The stress-strain curve and accompanying material properties for one of the specimens is shown in Figure 2.4. Yield stress was determined by 0.2 percent offset. The average tensile strength of the two specimens was 79.2 ksi.

Material properties of 4 x 8 in. concrete cylinders were also obtained. Cylinders were tested during the period that corresponding anchor specimens were tested. This period was usually 10 to 20 weeks after the concrete had been cast. In obtaining the stress-strain curve

and modulus of elasticity, two or more cylinders were instrumented with displacement transducers and were tested in uniaxial compression to failure. In determining the concrete compressive strength, three or more additional cylinders were tested and the results were averaged.

Because the concrete slabs were cast on five different occasions, there were five sets of slab specimens, each with distinct material properties. These specimens were classified into two groups, based on the concrete compressive strength. The first group, composed of three sets of slabs (A, B, and C), had cylinder compressive strengths of approximately 4500 psi. The other group, made up of the remaining two sets of slabs (D and E), had cylinder compressive strengths of approximately 6000 psi. Stress-strain curves for the five sets of slabs are presented in Figure 2.5. In the figure, average values of initial tangent modulus of elasticity and concrete compressive strength for each slab specimen set are reported.

2.3 Specimen Testing

2.3.1 Test Set-Up

The test set-up is illustrated in Figures 2.6 and 2.7. Subjecting the anchors to combined shear and tension loads required a loading apparatus that could apply load to the anchor in both the horizontal and vertical directions. This loading apparatus was composed of two elements: (1) a longitudinal member made up of two steel box sections and (2) a transverse beam made up of two steel channels connected together by welded steel plates. The longitudinal member was welded to the web of the transverse beam at its midspan. The transverse beam rested on roller supports located 36 in. apart on the slab surface. The loading apparatus was connected to two hydraulic rams. A horizontal ram was mounted to the longitudinal member of the apparatus and applied shear load to the anchor, while a second ram rested on top of the loading apparatus above the anchor and applied tension load.

Shear load applied by the horizontal ram was transferred to the anchor by a steel plate welded to the bottom of the loading apparatus, as shown in Figure 2.7. The diameter of the hole in the plate was 1/16 in. larger than that of the anchor bolt. When the hole became elongated, usually after several tests, the plate was replaced. A gap of about 3/8 in. existed between the bottom of the plate and the concrete surface. By maintaining this gap and having the loading apparatus rest on roller supports, frictional losses in the horizontal loading system were minimized.

The vertical ram applied tension to the anchor by means of a threaded rod which was attached to the anchor by a coupler. Because the ram rested on the top of the loading apparatus, it moved horizontally with the anchor as the anchor and the loading apparatus were displaced laterally by the shear ram. Due to the gap between the loading plate and the concrete surface, the tension load reaction was transferred to the slab at the roller supports.

To prevent the slab from displacing laterally or overturning during testing, it was attached to a pair of floor beams which, in turn, were secured to the floor by four column stubs. The slab was post-tensioned to the top flanges of the floor beams at the corners. In addition, steel angles were mounted on the top flanges of the floor beams at the ends of the slab to prevent horizontal displacement of the slab.

2.3.2 Instrumentation

Test specimens were instrumented to measure applied loads and resulting displacements of the anchor specimen. Figure 2.8 shows the instrumentation of a typical specimen. The tension load was measured by a 50-kip capacity load cell placed on top of the vertical hydraulic ram. Another 50-kip capacity load cell, located at the end of the horizontal ram, measured the shear load applied to the anchor.

Displacement of the anchor specimen was measured by linear variable differential transformers (LVDTs). As indicated in Figure 2.8, six LVDTs were employed to determine the displacement of the anchor bolt in the vertical and horizontal directions. LVDT 01 was connected to the top of the threaded rod and measured the vertical displacement of the anchor bolt and threaded rod in addition to uplift of the slab. Slab uplift was also measured by LVDT 03, which was placed underneath the center of the slab. Vertical displacement of the anchor bolt and threaded rod was then taken as the difference between the two LVDT readings.

The horizontal displacement of the anchor bolt was obtained by evaluating the difference between the readings of LVDT 04 and LVDT 02. LVDT 04 measured the horizontal displacement of both the anchor bolt and slab by means of a wire which looped around the shank of the anchor, whereas LVDT 02 measured the horizontal displacement of the slab only. A verification of the horizontal anchor displacement was provided by the horizontal ram's internal LVDT, which measured the ram stroke. Because ram stroke included the displacement of the beam and column assembly which the ram reacted against, LVDT 05 was placed behind the assembly to record this displacement. The difference between these two readings gave a measure of horizontal anchor displacement which was comparable to the reading of LVDT 04.

2.3.3 Test Procedure

The following testing procedure was used: an increment of load was applied to the anchor, readings from the instruments were recorded by computer, and the specimen was inspected for cracking or spalling. This process was repeated until the anchor could no longer sustain an increase in load. The test duration was usually about one hour.

The manner in which load increments were applied depended on the type of loading. For combined shear and tension loading, an increment of tension load was first applied, followed by a corresponding increment

in shear load. The relative magnitude of tension and shear load increments corresponded to the angle of inclination of applied load. For pure tension loading, the horizontal ram was not activated and load was applied solely by the vertical ram. For pure shear loading, load increments were provided solely from the horizontal ram; however, a small tension load (about 1 to 2 kips) was also applied to prevent the loading apparatus from overturning. The magnitude of load increments was usually equal to approximately 1 kip.

2.4 Summary

This chapter described the experimental program conducted to investigate the behavior of post-installed anchors subjected to static combined shear and tension loading. Twenty-four 1 in. diameter wedge-type expansion anchors were installed in holes drilled into uncracked slabs and were tested to failure. The details of the specimens, test set-up, and instrumentation were discussed. In Chapter 3 the results of the testing program are presented.

Table 2.1 Details of Testing Program

Specimen	f_c (psi) ¹	ϕ (deg.) ²	l_d (in.) ³
12	4350	0	4.00
27	4670	0	4.00
31	5950	0	4.00
33	5950	0	4.00
11	4350	0	5.25
17	4920	0	5.25
32	5950	0	5.25
28	4670	22.5	4.00
2	5950	45	3.50
15	4350	45	4.00
8	6350	45	4.50
13	4350	45	5.25
14	4350	45	5.25
9	6350	45	5.25
1	5950	45	6.00
20	4920	60	4.00
3	5950	60	4.00
18	4920	60	5.25
10	6350	60	5.25
19	4920	60	6.25
21	4670	70	4.00
23	4670	80	4.00
4	5950	90	3.00
24	4670	90	4.00

¹ f_c = compressive strength of 4 x 8 in. concrete cylinders

² ϕ = angle of inclination of applied load, measured with respect to a horizontal plane

³ l_d = anchor embedment depth, measured from concrete surface to bottom of wedge mechanism

Notes:

Anchor type: wedge-type expansion anchor

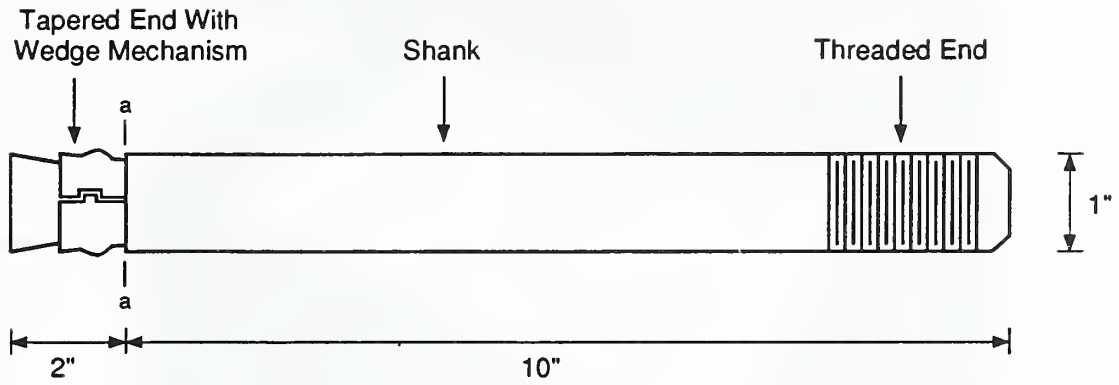
Anchor diameter: 1 in.

Edge distance: 15 in.

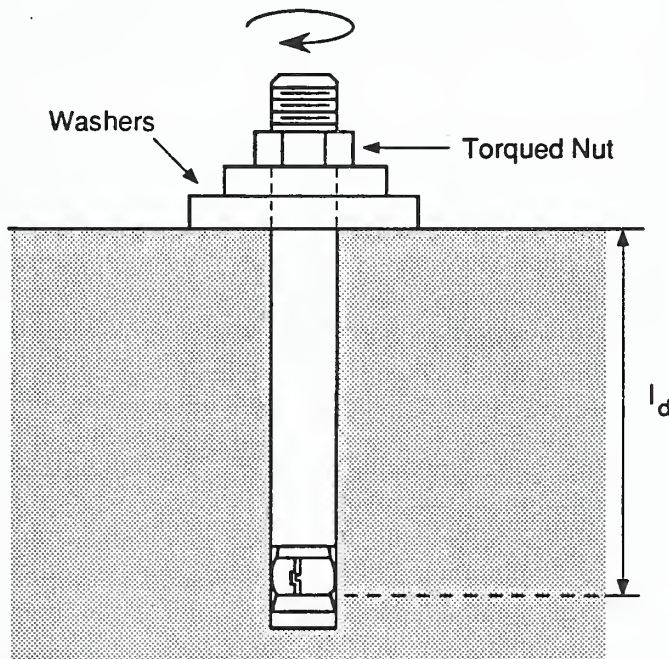
Concrete condition: uncracked

Anchor condition: no preload

Loading type: static



(a) Wedge-Type Expansion Anchor



(b) Installation of Anchor

Figure 2.1 Anchor Bolt Details

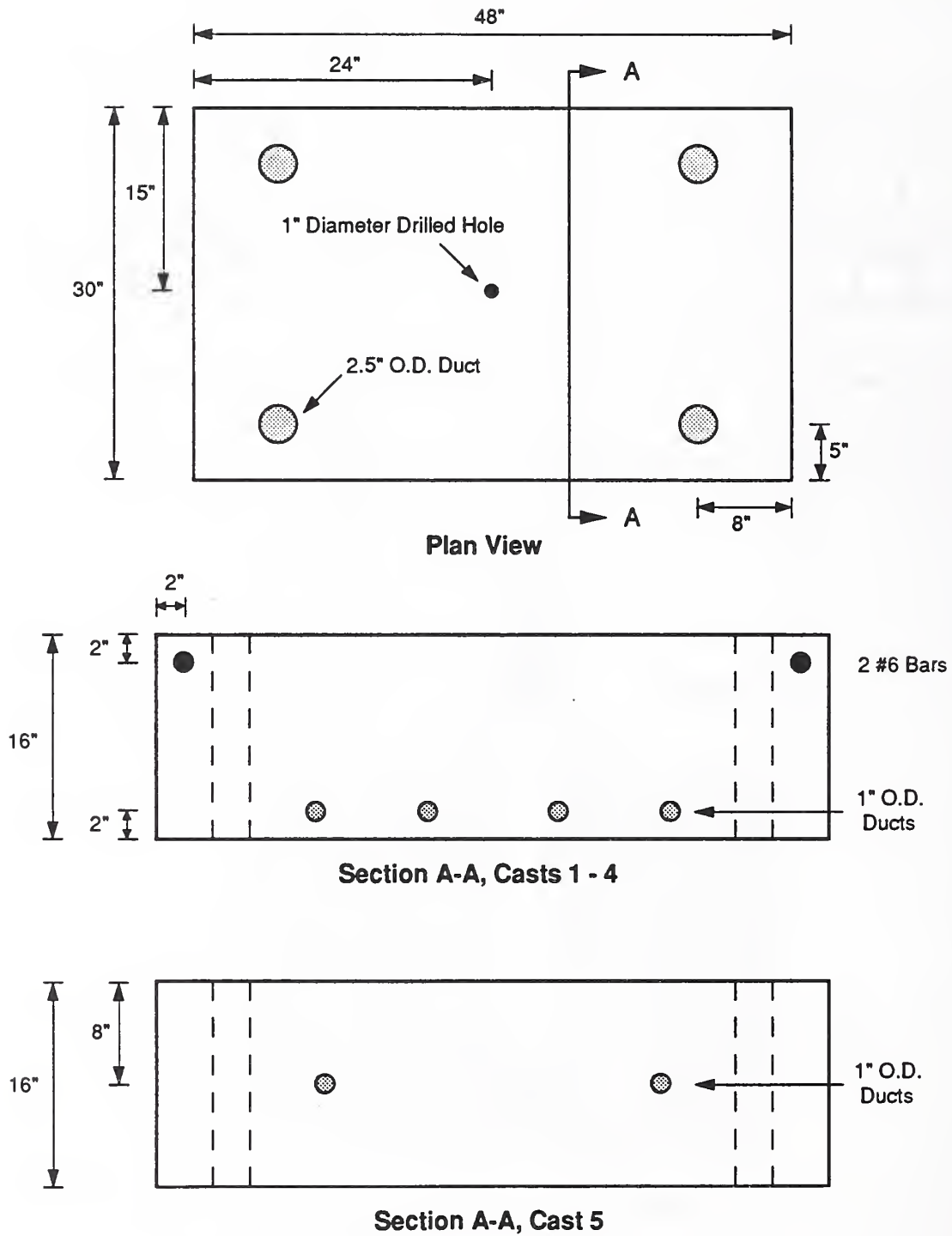


Figure 2.2 Concrete Slab Details

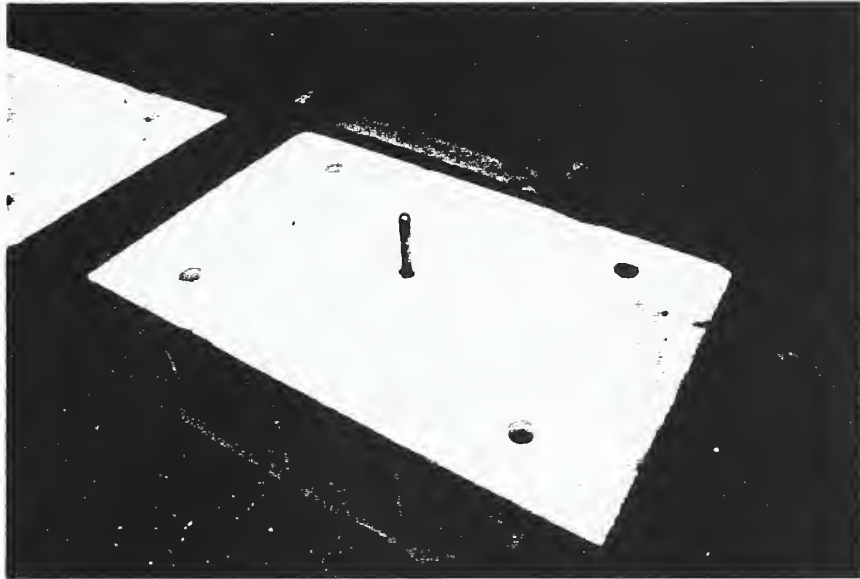


Figure 2.3 Fabricated Anchor Specimen

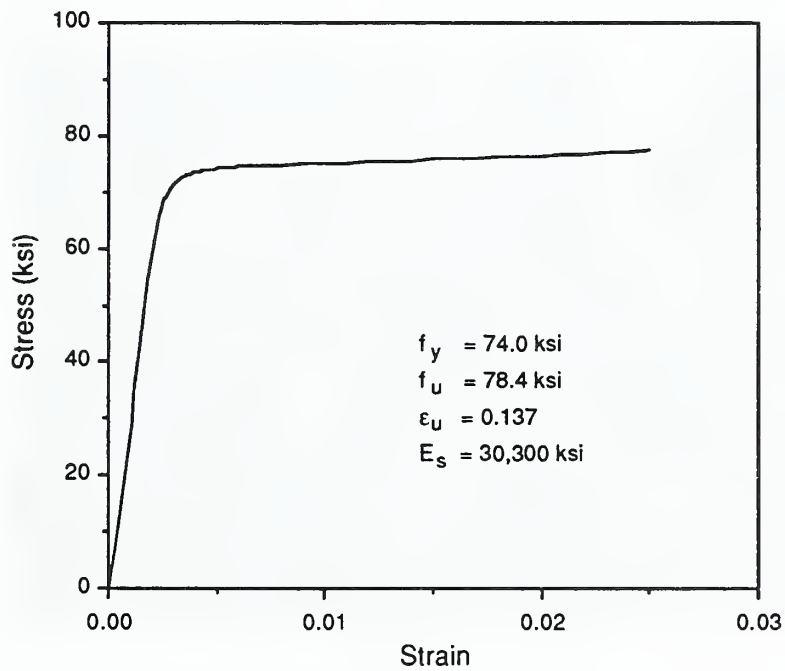
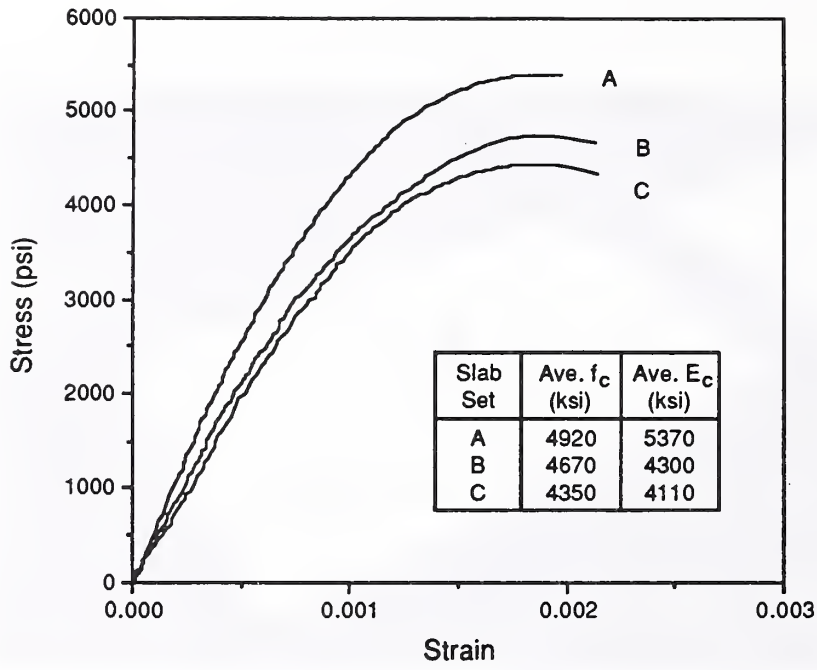
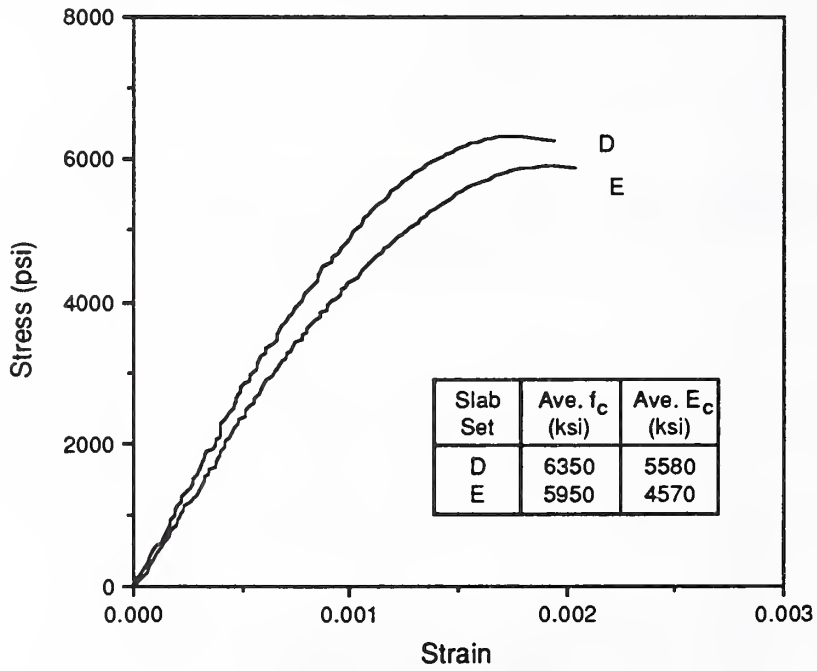


Figure 2.4 Stress-Strain Curve for Tensile Coupon of Wedge-Type Expansion Anchor



(a) Specimens With $f_c \approx 4500$ psi



(b) Specimens With $f_c \approx 6000$ psi

Figure 2.5 Stress-Strain Curves for Concrete Cylinders

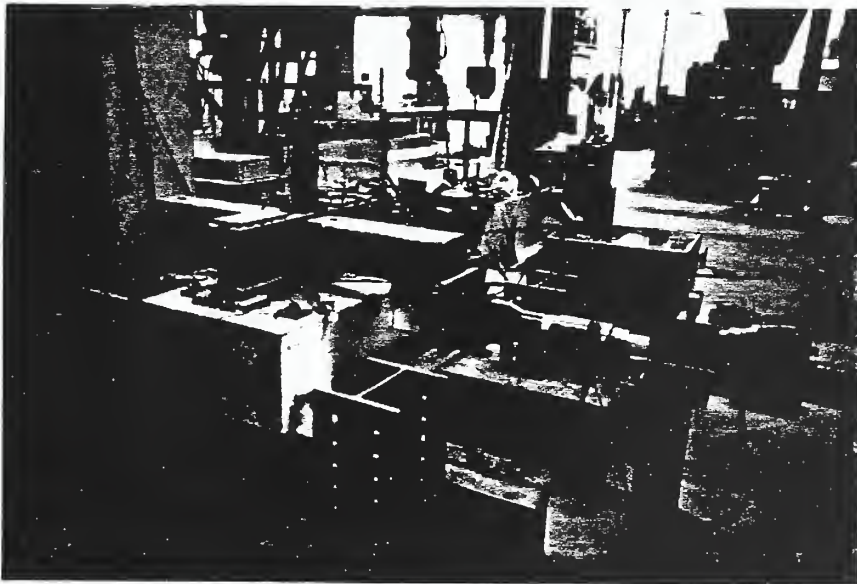
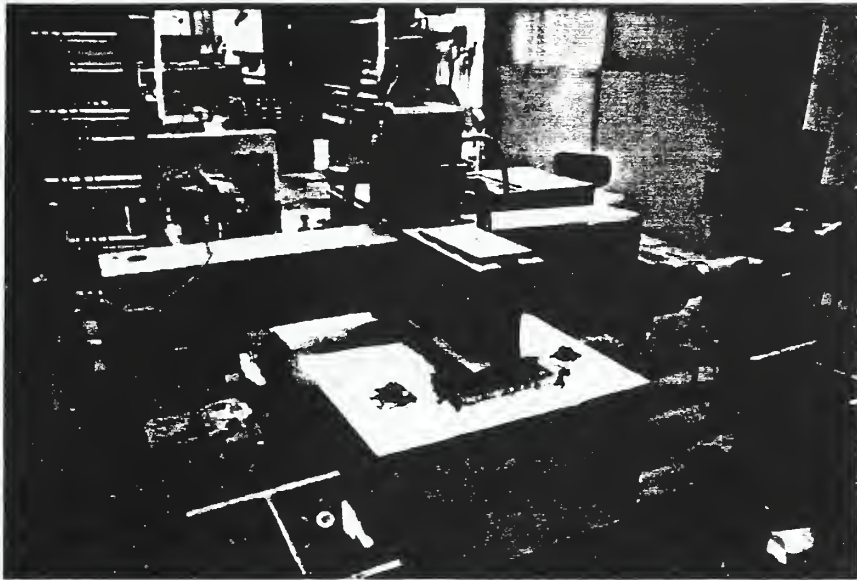


Figure 2.6 Test Set-Up

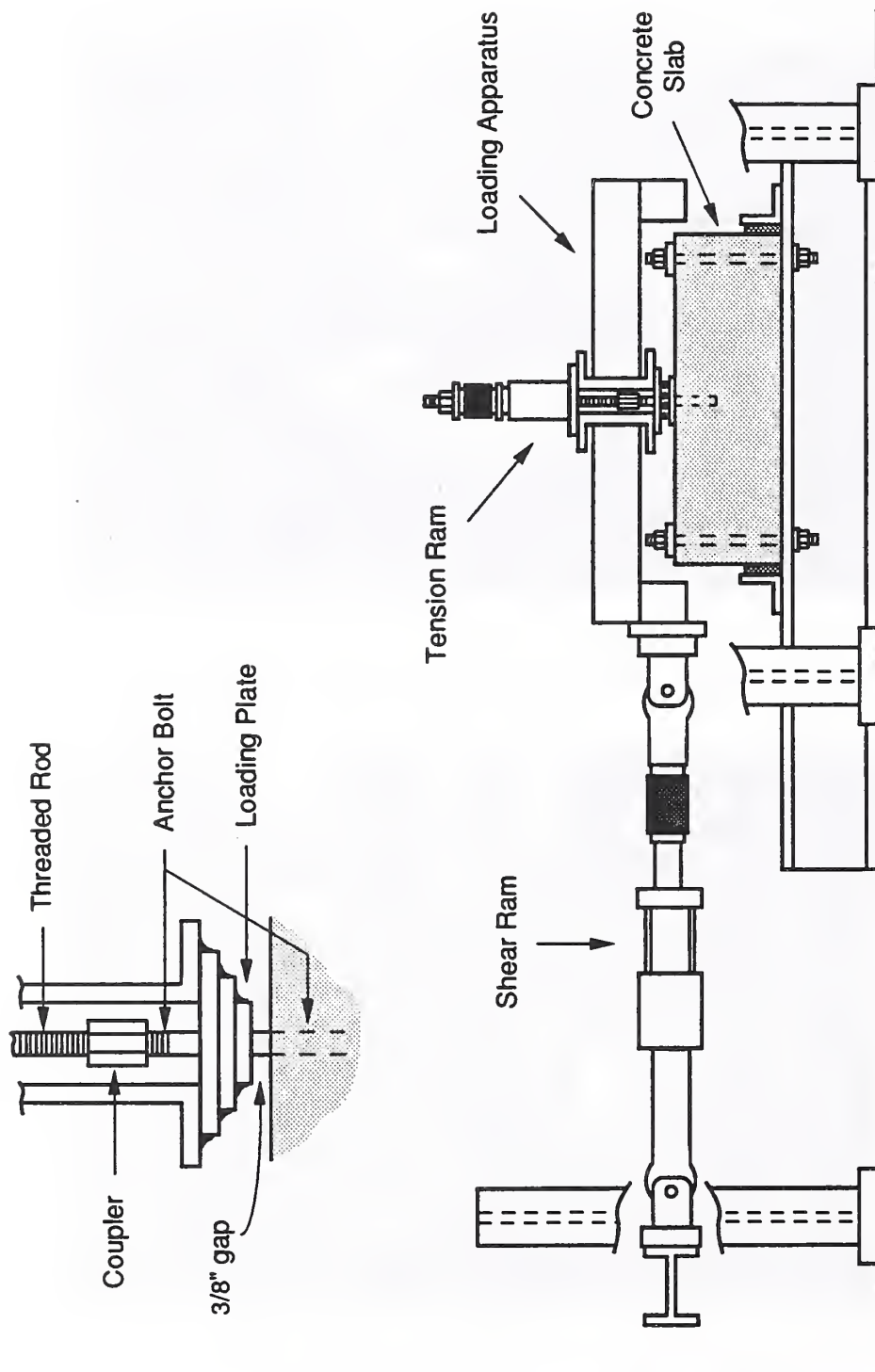


Figure 2.7 Details of Test Set-Up

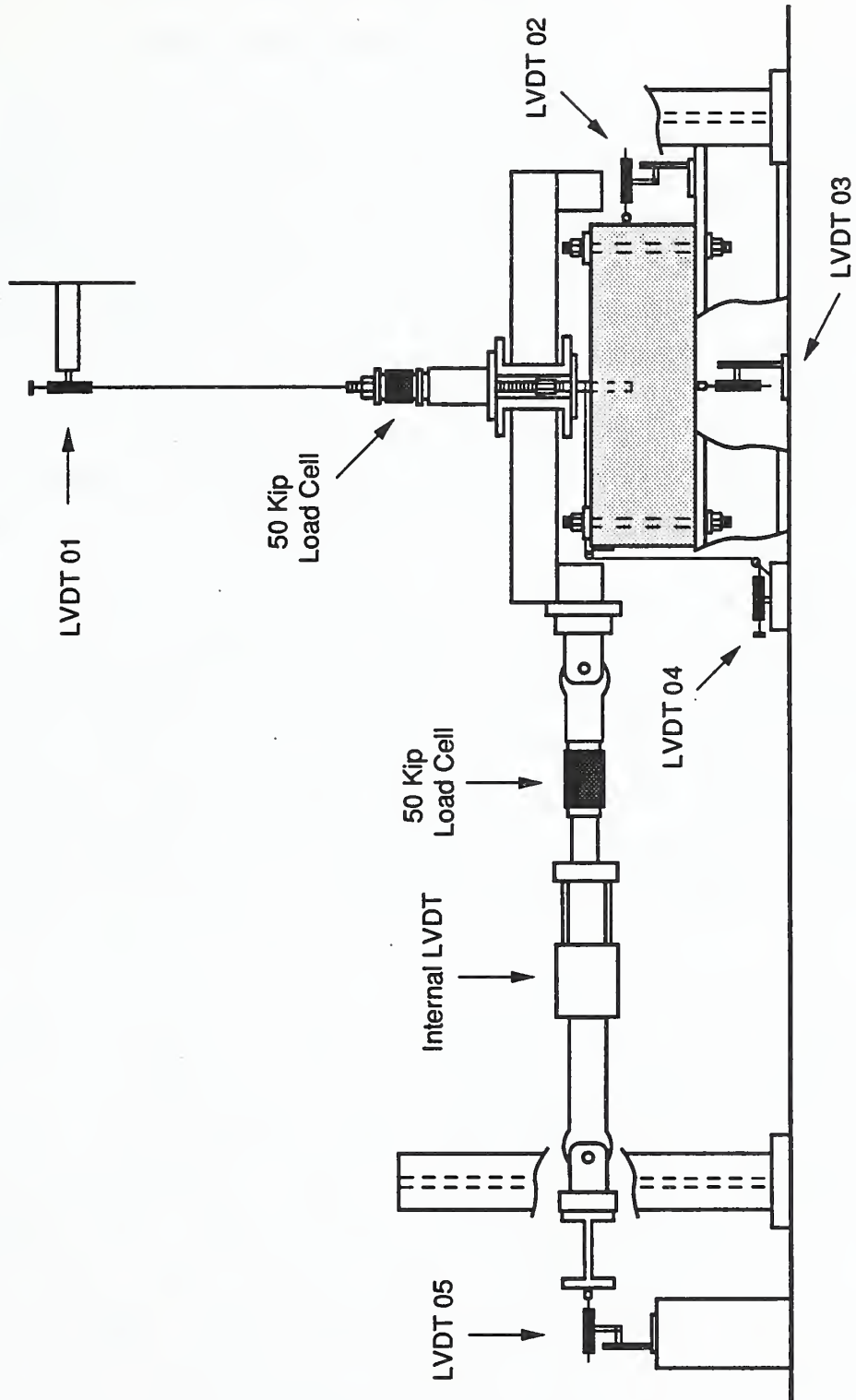


Figure 2.8 Instrumentation of Anchor Specimen

3.0 RESULTS OF EXPERIMENTAL PROGRAM

3.1 Ultimate Loads and Modes of Failure

The results of the testing program are summarized in Table 3.1. Specimens were divided into two groups according to the compressive strength of the concrete slabs in which anchors were embedded. The nominal concrete strengths of the two groups of specimens were 4500 and 6000 psi, respectively. (For simplicity, the nominal strength values will hereafter be used to denote specimen concrete strength.) Within each group, specimens were subdivided according to the angle of inclination of applied load (hereafter denoted as the load angle), ϕ , which varied from 0° (pure shear) to 90° (pure tension). For each load angle, one or more specimens with varying embedment depths were tested.

In Table 3.1, the terms V_u and T_u represent the ultimate shear and tension loads applied to the anchors, respectively. The mode of failure for each specimen is also reported. Four different failure modes were observed. Each mode was categorized according to which of the two load components, tension or shear, was the main cause of failure. Failures resulting primarily from the application of shear load were categorized as shear failures and failures resulting primarily from the application of tension load were categorized as tension failures.

Shear failures occurred in specimens tested at load angles between 0 and 60° . Figure 3.1 shows the loading condition for a typical anchor bolt. The applied shear load, V , caused the anchor to bear against the concrete, which led to compressive failure of the concrete and subsequent spalling. After spalling, the anchor continued to carry additional load until failure of the anchor occurred. As Figure 3.2 illustrates, there were two types of shear failures: steel fracture along the shank of the anchor and steel fracture at the reduced section of the anchor (section a-a in Figure 2.1(a)). Because the anchor was not located near the side of the slab, no failures occurred involving breakout of concrete in the shape of a partial cone.

Tension failures occurred in specimens tested at load angles between 60 and 90°. As depicted in Figure 3.3, two types of tension failures were observed: steel fracture at the threaded end of the anchor and cone-shaped tensile failure of the concrete. Steel fracture at the threads occurred in one specimen with $\phi = 60^\circ$. Cone-shaped failure of the concrete occurred for specimens with $\phi = 70$ to 90° . No anchors failed by pulling out of the hole; this result is probably attributable to the fact that all anchors, except for Specimen 4, satisfied the manufacturer's minimum embedment depth requirement of 3-1/2 in.

3.2 Behavior of Anchor Specimens

3.2.1 Specimens With $\phi = 0^\circ$

The behavior of specimens subjected to pure shear loads was variable. The two specimens with $l_d = 4.0$ in. and $f_c \approx 4500$ psi, shown in Table 3.1(a), had widely different ultimate capacities. Specimen 27 failed at 34.0 kips, while Specimen 12 failed at only 15.4 kips. The premature failure of Specimen 12 was most likely due to improper installation of the anchor. The load-displacement curves for Specimens 27 and 12 also differed. As indicated in Figure 3.4(a), Specimen 27 failed after substantial horizontal anchor displacement, while Specimen 12 failed without significant displacement. The curve for Specimen 27 was characterized by a yield plateau at approximately 25 kips in which the anchor deflected without an increase in shear load.

Both Specimens 12 and 27 failed in shear as a result of steel fracture at the reduced section. Figure 3.5 shows this failure for Specimen 27. The failure surface of the anchor, shown in Figure 3.5(b), was not along a horizontal plane, indicating that the steel failed as a result of combined shear and bending stresses. Evidence of yielding is observed in Figure 3.5(a) by the bent shape of the anchor. Yielding occurred when concrete surrounding the anchor spalled and permitted the anchor to bend over. The small amount of spalling around the anchor indicated that the failure was localized.

Variability in anchor behavior was also observed for the two specimens with $l_d = 4.0$ in. and $f_c \approx 6000$ psi. As Table 3.1(b) indicates, Specimens 31 and 33, identical in all respects, failed at 28.1 kips and 37.3 kips, respectively. Both anchors exhibited significant yielding deformation at approximately 25 kips, similar to that of Specimen 27 (see Figure 3.4(a)); however, Specimen 33, which displaced horizontally nearly twice as much as Specimen 31, failed as a result of steel fracture at the shank instead of at the reduced section. The shank failure of Specimen 33 is shown in Figure 3.6. The failure surface of the anchor was along a horizontal plane and was relatively smooth, indicating that the steel failed primarily due to shear stresses. The capacity of an anchor failing at the shank due to pure shear stresses without bending is:

$$F_u = f_{us} \times A_s \quad (1)$$

where

$$f_{us} = \text{steel shear strength} = .60 f_{ut}$$

$$A_s = \text{cross sectional area of anchor at shank} = \pi/4 D^2$$

The nominal shear strength value of $0.60 f_{ut}$ was recommended in the AISC Manual of Steel Construction[8]. With $f_{ut} =$ measured steel tensile strength = 79.2 ksi and $D =$ anchor diameter = 1 in., the equation yields $F_u = 37.3$ kips. The shear capacity of Specimen 33 was identical to this theoretical strength, indicating that bending stresses in the anchor were negligible.

The behavior of anchors with $l_d = 5.25$ in. was less variable than that of anchors with $l_d = 4.0$ in. The two specimens with $f_c \approx 4500$ psi, 11 and 17, had nearly identical ultimate capacities, although they experienced different modes of failure and, as indicated in Figure 3.4(b), had different load-displacement curves. Specimen 17 displayed the yielding behavior observed in the specimens with $l_d = 4.0$ in.

The influence of concrete strength on anchor behavior was not significant. Except for Specimen 12, specimens with $l_d = 4.0$ in.

showed large horizontal displacement at approximately 25 kips (see Figure 3.4(a)) and had similar capacities, regardless of the concrete strength. Specimens 27 and 33, in fact, had almost identical ultimate strengths and load-displacement curves. The behavior of anchors with $l_d = 5.25$ in. was also not strongly influenced by concrete strength. Although Specimen 32 with $f_c \approx 6000$ psi followed a different load-displacement path than Specimens 11 and 17 with $f_c \approx 4500$ psi (see Figure 3.4(b)), all three specimens had similar ultimate loads and horizontal displacements.

The effect of embedment depth on anchor behavior was also evaluated. As the embedment depth increased from 4.0 to 5.25 in., the ultimate shear load decreased slightly for specimens with $f_c \approx 4500$ psi (excluding Specimen 12) and increased slightly for specimens with $f_c \approx 6000$ psi. Figure 3.7 presents load-displacement curves showing embedment depth as a variable. As the figure indicates, anchor deformation was not significantly affected by the increase in embedment depth at either concrete strength. At $f_c \approx 4500$ psi, Specimens 17 and 27 followed nearly identical load-displacement paths. At $f_c \approx 6000$ psi, the load-displacement curve for Specimen 32 with $l_d = 5.25$ in. was similar in shape to those for Specimens 31 and 33 with $l_d = 4.0$ in. even though it displayed yielding behavior at a higher shear load.

In summary, the behavior of anchors subjected to pure shear loads was not significantly affected by either concrete strength or embedment depth in the range in which they varied. In addition, anchor behavior was variable. Specimens with identical embedment depths and concrete strengths followed different load-displacement paths, failed at different loads, and experienced different modes of failure. Even anchors which had identical failure modes had different capacities.

Despite this variability in behavior, all the specimens except for 12 followed a similar pattern of behavior. Anchor displacements were initially relatively small and the load-displacement curves were approximately linear. This linear displacement response corresponded to

bearing of the anchor against the side of the hole. Further application of shear load resulted in concrete spalling at shear loads ranging between 10 and 18 kips. Spalling increased the moment arm of the applied shear load. As a result, the load-displacement curves became nonlinear as anchor displacements increased significantly due to bending of the anchor.

Further application of shear load above that which caused spalling eventually resulted in steel fracture of the anchor due to the combined effects of shear and bending stresses. In general, anchors failing at the reduced section had lower capacities than anchors failing at the shank due to the smaller cross sectional area of the reduced section and to the larger bending stresses at the reduced section. The presence of bending stresses resulted in different capacities for anchors with identical modes of steel failure. Because horizontal anchor displacements varied between identical specimens, bending stresses in each anchor were unique, resulting in different stress distributions for each anchor. In Specimen 33, however, bending stresses were negligible and the anchor reached the limiting shear capacity.

3.2.2 Specimen With $\phi = 22.5^\circ$

One specimen was tested at a load angle of 22.5° ($T/V = 0.41$). The horizontal and vertical components of the load-displacement curve are shown in Figure 3.8. In Figure 3.8(a), load is expressed in terms of the horizontal (shear) component of the total applied load and displacement is represented by the corresponding horizontal anchor displacement. In Figure 3.8(b), load is expressed in terms of the vertical (tension) component of the total applied load and displacement is represented by the corresponding vertical anchor displacement.

The vertical anchor displacement in Figure 3.8(b) consisted of contributions from three main sources: elongation of the threaded coupling rod, elongation of the anchor, and slip of the tapered end of the anchor over the wedge mechanism. Elongation of the threaded rod was

determined by calibration tests and is indicated in Figure 3.8(b) as a dashed line. The vertical displacement of the anchor bolt alone, then, which consisted of elongation and slip of the anchor, was equal to the difference between the load-displacement curve and the dashed line. Because the magnitude of anchor elongation was only about one tenth of the threaded rod elongation, it was considered to be negligible. The vertical displacement of the anchor bolt was thus primarily due to slip.

Specimen 28 failed in shear as a result of steel fracture at the reduced section at an applied shear load of 25.7 kips, as indicated in Table 3.1(a). Figure 3.8(a) shows that the anchor initially experienced a slight nonlinear horizontal displacement as the anchor moved to the side of the hole. Horizontal displacement then increased approximately linearly up to a shear load of 20 to 22 kips, at which point the anchor began to displace significantly prior to failure. As was noted in the specimens with $\phi = 0^\circ$, this nonlinear displacement started to occur soon after concrete spalling was first observed.

The magnitude of vertical displacement of the anchor was small. As shown in Figure 3.8(b), the vertical component of the load-displacement curve closely followed the dashed line until the applied tension load reached approximately 10 kips, indicating that vertical displacement initially consisted solely of elastic deformation of the threaded rod and anchor. At 10 kips, the curve diverged from the dashed line, representing the beginning of anchor slip. The fact that slip did not begin until the applied load reached 10 kips is due to the effect of the preload applied to the anchor during installation. Although the preload was released prior to testing, it seated the wedge mechanism in the hole, preventing anchor slip until the applied tension load became sufficiently large.

3.2.3 Specimens With $\phi = 45^\circ$

Anchor specimens tested at a load angle of 45° ($T/V = 1.0$) were subjected to equal magnitudes of tension and shear; however, they failed

as a result of the application of the shear load component. Therefore, the shear component of the total load dominated anchor behavior.

As was observed in the specimens subjected to pure shear load, the behavior of specimens with $\phi = 45^\circ$ was variable. Table 3.1(a) shows that Specimens 13 and 14, which were identical in all respects, failed at different shear loads (27.3 and 33.9 kips, respectively) and experienced different modes of failure. The horizontal components of the load-displacement curves for Specimens 13 and 14, presented in Figure 3.9, were also different, even though the two specimens had nearly identical ultimate horizontal displacements.

The effect of concrete strength on anchor behavior was not significant. At an embedment depth of 5.25 in., the behavior of Specimens 13 and 14 with $f_c \approx 4500$ psi was almost identical to that of Specimen 9 with $f_c \approx 6000$ psi. As indicated in Table 3.1, the ultimate shear load of Specimen 9 was only 2% larger than the average ultimate shear load of Specimens 13 and 14. Figure 3.9 shows the load-displacement behavior for specimens with $l_d = 5.25$ in. The shapes of the horizontal components of the load-displacement curves for Specimens 9 and 14 were similar, showing that concrete strength did not have much effect on load-displacement behavior.

Embedment depth had a strong effect on the ultimate behavior of anchor specimens. For specimens with $f_c \approx 4500$ psi shown in Table 3.1(a), increasing the embedment depth from 4.0 to 5.25 in. resulted in an increase in ultimate shear load from 17.8 to an average of 30.6 kips and in a change in failure mode from anchor fracture at the reduced section to fracture at the shank. For specimens with $f_c \approx 6000$ psi indicated in Table 3.1(b), increasing the embedment depth from 3.5 to 6.0 in. resulted in an increase in ultimate shear load from 16.1 to 39.4 kips. The failure mode also changed from anchor fracture at the reduced section for specimens with $l_d = 3.5$ and 4.5 in. to fracture at the shank for specimens with $l_d = 5.25$ and 6.0 in.

The effect of embedment depth on anchor capacity is illustrated in Figure 3.10. Anchor capacity is expressed in terms of the ultimate shear load, V_u . The dashed horizontal line indicates the limiting shear strength of the anchor corresponding to failure at the shank due to pure shear stresses (see Equation (1)). Because concrete strength did not significantly influence anchor behavior, all specimens were plotted together.

The plot indicates that anchor capacity increased approximately linearly with increasing embedment depth. Specimen 1 with $l_d = 6.0$ in. reached the limiting shear capacity. (In fact, Specimen 1 exceeded the theoretical shear strength by 5.6%. This discrepancy is likely due to the fact that, during testing, the loading plate of the loading apparatus shown in Figure 2.7 was forced down against the concrete surface, resulting in significant frictional losses in the horizontal loading system.) Embedding anchors at a depth greater than 6.0 in., then, would not be expected to further increase the shear capacity. The plot also indicates that the failure mode changed from steel fracture at the reduced section to fracture at the shank at an embedment depth of 5.25 in. and that anchors which fractured at the shank had higher capacities than those failing at the reduced section.

Anchor deformation was also influenced by embedment depth. Figure 3.11 presents load-displacement curves for specimens with $f_c \approx 6000$ psi. In Figure 3.11(a), specimens followed nearly identical linear horizontal load-displacement paths up to a shear load of approximately 10 kips. As the load increased above 10 kips, the curves became nonlinear and diverged from each other. The load at which the curves became nonlinear increased as the embedment depth increased. Consequently, the horizontal displacement at a given magnitude of shear load decreased as the embedment depth increased.

Vertical anchor displacement was similarly influenced by embedment depth. As Figure 3.11(b) illustrates, specimens initially followed linear load-displacement paths corresponding to elongation of the

threaded rod. As the tension load increased, the curves eventually became nonlinear and diverged from the dashed line, indicating the beginning of anchor slip. The load at which anchor slip began increased from 8 to 24 kips as the embedment depth increased from 3.5 to 6.0 in. Consequently, the magnitude of vertical displacement at a given tension load decreased as the embedment depth increased. The curves for Specimens 1 and 9 also showed a sudden increase in slope prior to failure. This phenomenon was due to the large horizontal displacement of these anchors, which caused the upper end of the anchors to move downward and result in an apparent decrease in vertical displacement.

The reliance of anchor behavior on embedment depth is attributable to the manner in which the anchor participated in the load-carrying process. Increasing the embedment depth allowed the anchor to transfer the applied shear load to the concrete by bearing over a larger surface area, resulting in smaller bearing stresses in the concrete. Therefore, as the embedment depth increased, concrete spalling initiated at a higher load. The delay in spalling for more deeply embedded anchors delayed the start of nonlinear load-displacement response, as Figure 3.11(a) indicates. Increasing the embedment depth also decreased the maximum depth of spalled concrete. (The maximum depth of spalling is defined in Figure 3.1.) Table 3.2 shows that the maximum depth of spalling decreased from 2.5 to 0.5 in. as the embedment depth increased from 3.5 to 6.0 in. This decrease in spalling depth for more deeply embedded anchors resulted in a smaller moment arm of the applied shear load and thus less bending of the anchor.

Bending stresses in the anchors combined with shear and tensile stresses to cause fracture of the anchor. As the embedment depth increased, the magnitude of bending stresses in the anchor decreased, resulting in an increased capacity (see Figure 3.10). The limiting capacity indicated in Figure 3.10 represented anchor steel shear failure at the shank without bending (or tensile) stresses. Because Specimen 1 with $l_d = 6.0$ in. reached this limit, its depth can be considered as the critical depth at which bending stresses did not affect anchor capacity.

Embedment depth also influenced the failure mode. For anchors with shallow embedment depths in which the depth of spalling was relatively large, the tapered end of the anchor was required to transfer part of the applied shear load to the concrete. Because of its reduced cross sectional area, it provided less resistance than the shank. In addition, the bending moment at the reduced section was much larger than that at the shank. Consequently, anchors with relatively small embedment depths fractured at the reduced section. However, as the embedment depth increased and the reduced section became located farther away from the concrete surface, the failure mode changed to fracture at the shank. Anchors which failed at the reduced section had lower capacities than otherwise identical anchors failing at the shank.

In summary, increasing the embedment depth increased the anchor capacity and changed the mode of failure from steel fracture at the reduced section to fracture at the shank. This transition in failure mode occurred at an embedment depth of 5.25 in. Increasing the embedment depth also increased the load at which the horizontal and vertical components of the load-displacement curves became nonlinear.

3.2.4 Specimens With $\phi = 60^\circ$

The applied tension load had a measurable effect on the behavior of specimens tested at a load angle of 60° ($T/V = 1.73$). One specimen, in fact, failed in tension. Anchor behavior, then, experienced a transition from shear-dominant (for specimens with $\phi = 0$ to 45°) to tension-dominant (for specimens with $\phi = 70$ to 90°) at a load angle of approximately 60° .

Similar to specimens with $\phi = 0$ to 45° , the effect of concrete strength on anchor behavior was insignificant. For a given embedment depth of 4.0 or 5.25 in., the shear capacity increased only slightly as the concrete strength increased from 4500 to 6000 psi and the failure mode (anchor fracture at the reduced section) did not change. Anchor deformation was similarly unaffected by concrete strength. Figure 3.12

presents the horizontal components of the load-displacement curves for specimens with $l_d = 4.0$ and 5.25 in. At both embedment depths, the curves were not significantly affected by concrete strength.

The embedment depth, on the other hand, had a strong effect on anchor behavior. As indicated in Table 3.1(a), the ultimate shear load increased from 15.4 to 26.3 kips as the embedment depth increased from 4.0 to 6.25 in. for specimens with $f_c \approx 4500$ psi. At $f_c \approx 6000$ psi, the ultimate shear load similarly increased as the embedment depth increased (see Table 3.1(b)). In addition, the failure mode changed from anchor fracture at the reduced section to anchor tensile fracture at the threads at an embedment depth of 6.25 in. Figure 3.13 shows this tension failure for Specimen 19.

The change in failure mode from shear to tension was a result of the effect of the magnitude of applied tension load. For a load angle of 60° , the magnitude of tension load was 1.73 times that of the shear load. Thus, at a given shear load, the tension load was 1.73 times larger for specimens with $\phi = 60^\circ$ than for specimens with $\phi = 45^\circ$. Specimen 19, which had a large embedment depth (and thus a high shear capacity), could then reach the limiting anchor tension capacity. The limiting tension capacity is:

$$F_{ut} = f_{ut} \times A_{net} \quad (2)$$

where

$$f_{ut} = \text{steel tensile strength} = 79.2 \text{ ksi}$$

$$A_{net} = \text{cross sectional area of threads} = \pi/4 (D - .9743/n)^2$$

With $D = \text{anchor diameter} = 1$ in. and $n = \text{number of threads per inch} = 8$, the limiting capacity is $F_{ut} = 48.0$ kips. Specimen 19 failed in tension at $T_u = 46.0$ kips which is within 4% of the theoretical value.

The effect of embedment depth on anchor capacity is illustrated in Figure 3.14. Anchor capacity is expressed in terms of the ultimate shear load, V_u . Because concrete strength did not have a measurable

effect on anchor behavior, all specimens were plotted together. The limiting applied shear load corresponding to the tensile capacity calculated in Equation (2) is represented by the dashed line and is equal to $F_{us} = F_{ut}/\tan 60^\circ = 27.7$ kips. The plot shows an approximately linear increase in anchor capacity with embedment depth. The embedment depth at which the failure mode changed to from shear to tension was between 5.25 and 6.25 in. Because the tension failure of Specimen 19 represented the limiting capacity of the anchor, anchors embedded deeper than this critical depth would not benefit in an increase in strength.

The effect of embedment depth on load-displacement behavior for specimens with $f_c \approx 4500$ psi is presented in Figure 3.15. Horizontal anchor displacement shown in Figure 3.15(a) was somewhat influenced by embedment depth. As was observed in specimens with $\phi = 45^\circ$, the load at which the load-displacement curves became nonlinear tended to increase with increasing embedment depth. Consequently, the horizontal displacement at a given load decreased as the embedment depth increased. This trend was disrupted, however, when Specimen 19 showed a peculiar jump in horizontal displacement at about 16 kips. A similar discontinuity is evident in the vertical displacement in Figure 3.15(b). During testing, this increase in displacement was accompanied by temporary loss of hydraulic pressure in both the horizontal and vertical loading rams. These observations indicate that the anchor probably slipped due to a reduction in concrete confinement.

Vertical anchor displacement was similarly influenced by embedment depth. As Figure 3.15(b) indicates, the paths of the load-displacement curves initially coincided with the dashed line, until at some value of tension load they diverged from it, indicating the beginning of anchor slip. The tension load at which anchor slip began increased from approximately 13 kips to 17 kips as the embedment depth increased from 4.0 to 6.25 in. In addition, the anchor slip load corresponded almost identically to the load at which the horizontal load-displacement curves became nonlinear (which indicated the beginning of concrete spalling).

The reliance of the anchor slip load on embedment depth is likely attributable to spalling of the concrete. Prior to spalling, some of the applied tension load was transferred to the concrete by friction along the shank due to the action of the shear load in bearing the anchor against the hole wall. Transfer of the tension load by friction effectively increased the load at which anchor slip began, since less tension load was being transferred at the wedge mechanism. However, when spalling occurred, the friction transfer mechanism along the shank diminished, often sufficiently increasing the magnitude of tension load transferred at the wedge to initiate anchor slip. Because the load at which spalling occurred increased with increasing embedment depth, the anchor slip load also increased with increasing embedment depth.

In summary, increasing the embedment depth increased anchor strength and changed the failure mode from shear to tension. The embedment depth at which the failure mode changed was between 5.25 and 6.25 in. Increasing the embedment depth also tended to increase the load at which the horizontal and vertical load-displacement curves became nonlinear.

3.2.5 Specimens With $\phi = 70$ to 90°

The behavior of specimens tested at load angles of 70 to 90° was dictated by the magnitude of applied tension load. All the specimens with $\phi = 70$ to 90° failed in tension, whereas only one specimen with $\phi \leq 60^\circ$ failed in tension. Specimens with $f_c \approx 4500$ psi had embedment depths of 4.0 in., while the specimen with $f_c \approx 6000$ psi had an embedment depth of 3.0 in. Therefore, the effects of embedment depth and concrete strength could not be isolated.

All specimens experienced cone-shaped tensile failure of the concrete. However, in Specimens 21, 23, and 24 with $f_c \approx 4500$ psi, the cone-shaped mass of concrete was broken, whereas the concrete cone of Specimen 4 with $f_c \approx 6000$ psi was unbroken. The broken failure cone of

Specimen 23 is shown in Figure 3.16. The arrow in the upper photo indicates the direction of the applied shear load. The failure cone of Specimen 4 is presented in Figure 3.17. The angle of inclination of the conical failure surface with respect to the concrete surface was in the range of 30 to 45° for Specimens 21, 24, and 4 and 20 to 45° for Specimen 23.

The load angle did not have much influence on the ultimate tensile capacity, T_u , for specimens with $f_c \approx 4500$ psi and $l_d = 4.0$ in. As indicated in Table 3.1(a), the tensile capacity ranged between 23.9 and 26.5 kips as the load angle increased from 70 to 90°, a change of about 11%. The combined effects of concrete strength and embedment depth were assessed by comparing Specimens 24 and 4, which were both subjected to pure tension. Specimen 24, which had a larger embedment depth and lower concrete strength than Specimen 4, had a higher capacity, indicating that the increase in embedment depth raised the capacity more than the decrease in concrete strength lowered it.

The strengths of the two specimens subjected to pure tension were compared with values obtained from predictive equations proposed by Eligehausen[9] and ACI Committee 349[10]. Eligehausen tested in tension approximately 2000 anchors with bolt diameters ranging from 0.20 to 0.94 in. Based on this study, an equation was developed to predict anchor tensile capacity for cone-shaped failure of the concrete:

$$F_{ut} = 8.7 l_d^{1.54} f'_c{}^{2/3} \quad (1b) \quad (3)$$

where

- l_d = embedment depth measured from the concrete surface to the bottom of the wedge mechanism, in
- f'_c = specified concrete compressive strength, psi

The equation developed by ACI Committee 349 is based on the assumption that the average tensile stress along the concrete failure surface is $4\sqrt{f'_c}$ and that the failure surface is oriented at an angle

of 45° with respect to the concrete surface. The equation for tensile capacity for cone-shaped failure of the concrete is:

$$F_{ut} = 4\pi\sqrt{2} l_d^2 \sqrt{f'_c} \quad (1b) \quad (4)$$

Equation (3) yielded $F_{ut} = 20.6$ kips for Specimen 24 and 15.5 kips for Specimen 4. These values underestimated the measured capacities of 24.9 and 19.4 kips by 17% and 20%, respectively. Equation (4) yielded $F_{ut} = 19.4$ kips for Specimen 24 and 12.3 kips for Specimen 4, which underestimated the measured capacities by 22% and 37%, respectively. Neither equation predicted anchor strength accurately, although Equation (3) was somewhat more accurate than Equation (4).

Vertical components of the load-displacement curves are presented in Figure 3.18. For specimens with $f_c \approx 4500$ psi and $l_d = 4.0$ in. shown in Figure 3.18(a), the tension load at which the curves diverged from the dashed line, corresponding to the beginning of anchor slip, increased from 9 to 12 kips as the load angle decreased from 90° to 70° . As a result, the vertical displacement at a particular tension load decreased with decreasing load angle. In addition, the two specimens subjected to pure tension shown in Figure 3.18(b) followed almost identical load-displacement paths even though they had different concrete strengths and embedment depths. The load at which anchor slip began was approximately the same for both specimens (9 to 10 kips), indicating that neither concrete strength nor embedment depth influenced anchor slip in the absence of shear load.

In summary, the ultimate behavior of specimens with $\phi = 70$ to 90° was controlled by the magnitude of applied tension load. The capacity of the specimens was limited by the tensile strength of the concrete and all specimens exhibited cone-shaped failure of the concrete. The magnitude of applied shear load did not have a strong effect on anchor behavior.

3.2.6 Effect of Load Angle

The effect of load angle on behavior of anchor specimens was also investigated. Table 3.3 presents test results for specimens with embedment depths of 4.0, 5.25, and 6.0 to 6.25 in. in which the load angle was varied. (Specimen 12 was considered to be an anomaly due to its premature failure and was excluded from Table 3.3.) Because concrete strength had little influence on anchor behavior at load angles between 0 and 60°, specimens with $\phi \leq 60^\circ$ were not differentiated according to concrete strength.

The load angle had a strong effect on the failure mode. Specimens with $\phi \leq 60^\circ$ failed in shear, while specimens with $\phi \geq 60^\circ$ failed in tension. At $\phi = 60^\circ$, both shear and tension failures occurred. The failure mode, then, experienced a transition from shear to tension at a load angle of approximately 60°. For specimens failing in shear, the embedment depth at which failure changed from steel fracture at the reduced section to fracture at the shank increased as the load angle increased.

The load angle also influenced anchor capacity. As indicated in Table 3.3, the ultimate shear load, V_u , decreased as the load angle increased from 0 to 60° for specimens failing in shear. For specimens with $l_d = 4.0$ in., V_u decreased from an average of 33.1 to 16.2 kips as the load angle increased from 0 to 60°. For specimens with $l_d = 5.25$ in., V_u decreased from an average of 31.6 to 22.7 kips as the load angle increased from 0 to 60°. The effect of the tension load, then, was to decrease the shear capacity of anchors failing in shear. Specimens experiencing cone-shaped concrete tensile failures, on the other hand, were not adversely affected by the presence of shear load. The tension capacity, T_u , remained approximately constant as the load angle decreased from 90 to 70° for specimens with $l_d = 4.0$ in.

Although the load angle influenced the ultimate shear capacity, V_u , its effect on the resultant capacity, P_u (where $P_u = \sqrt{V_u^2 + T_u^2}$), was

not clearly defined. The effect of load angle on the resultant capacity is illustrated in Figure 3.19. Figure 3.19(a) indicates that, despite the large range in capacity (indicated by the shaded region), the resultant strength of specimens with $l_d = 4.0$ in. was not significantly influenced by the load angle as it increased from 0 to 90°. For specimens with $l_d = 5.25$ in., there was also a large range in resultant capacity, as shown in Figure 3.19(b) for load angles between 0 and 60°. The specimens with $\phi = 0^\circ$ had an unexpectedly low average resultant capacity of 31.6 kips (which was less than that of specimens with $\phi = 0^\circ$ and $l_d = 4.0$ in.). This average capacity was considerably less than that of specimens with $\phi = 45$ and 60° , which had nearly identical capacities.

The effect of load angle on anchor strength was also evaluated by examining the influence of embedment depth on capacity at different load angles. Figure 3.20(a) shows plots of anchor shear load capacity, V_u , versus embedment depth for specimens with $\phi = 45$ and 60° , taken from Figures 3.10 and 3.14. The plots indicate that, although the ultimate shear load increased linearly with increasing embedment depth at both load angles, the rate of increase was larger for specimens with $\phi = 45^\circ$. In Figure 3.20(b) these results are plotted again in terms of the resultant load capacity, P_u . This plot shows that the specimens with $\phi = 45$ and 60° had approximately the same linear increase in resultant capacity with embedment depth. Thus the resultant capacity was not significantly influenced as the load angle increased from 45 to 60°.

Figure 3.21 presents a plot of resultant capacity versus embedment depth for specimens with $\phi = 0$ to 90° , representing an expanded version of Figure 3.20(b). The results for all specimens in the testing program (except for Specimen 12) are plotted. The resultant capacity increased approximately linearly with embedment depth, independent of the load angle. However, at a given embedment depth, there was much variability in capacity, mostly originating from the specimens with $\phi = 0^\circ$. In particular, at $l_d = 5.25$ in., the capacities of the three specimens with $\phi = 0^\circ$ were much lower than the trend otherwise indicated. (These three

specimens are the same as those in Figure 3.19(b) which were observed to be lower in capacity than expected.)

Based on observations made in Figures 3.19 to 3.21, it is concluded that the resultant capacity was not significantly affected by load angle and that P_u increased approximately linearly with increasing embedment depth. The scope of these observations are, however, limited to concrete strengths in the range of 4500 to 6000 psi. Although anchor capacity was found to be unaffected by concrete strength when shear failure controlled, the capacity of specimens experiencing cone-shaped concrete tensile failure is affected by concrete strength. Consequently, it is unlikely that the results for specimens tested at load angles of 70 to 90° and having concrete strengths outside the range of 4500 to 6000 psi would fit the trend in Figure 3.21.

The effect of load angle on anchor deformation was also evaluated. Figures 3.22 and 3.23 present load-displacement curves for specimens with nominal concrete strengths of 4500 psi and embedment depths of 4.0 and 5.25 in., respectively. For specimens with $l_d = 4.0$ in. in Figure 3.22, the full range of load angle ($\phi = 0$ to 90°) was examined. For specimens with $l_d = 5.25$ in. in Figure 3.23, the load angle ranged between 0 and 60°. Load-displacement curves for specimens with nominal concrete strengths of 6000 psi were not included; however, load-displacement behavior of specimens with $f_c \approx 6000$ psi was found to be similar to that of specimens with $f_c \approx 4500$ psi for $\phi \leq 60^\circ$.

For specimens with $l_d = 4.0$ in., the load angle had a marked effect on horizontal anchor deformation. As Figure 3.22(a) indicates, the ultimate horizontal displacement decreased with increasing load angle. The ultimate displacement of Specimen 27 with $\phi = 0^\circ$ was approximately 4 times greater than the next largest ultimate displacement. Specimen 27 also displayed yielding behavior which was not evidenced in any of the other specimens.

Figure 3.22(a) also shows that the load at which the load-displacement curves became nonlinear decreased with increasing load angle. This trend was due to the fact that concrete spalling, which allowed the anchor to bend over and displace horizontally, occurred at lower shear load values as the load angle increased, as shown in Table 3.4(a). The dependence of the spalling load on the load angle resulted from the interaction between bearing stresses induced in the concrete by the shear load and confining stresses around the wedge mechanism at the bottom of the anchor. As the magnitude of tension load increased with increasing load angle, the magnitude of the confining stresses increased, which, when combined with the bearing stresses, resulted in a decreased spalling load.

The load angle also influenced vertical anchor displacement of specimens with $l_d = 4.0$ in. As shown in Figure 3.22(b), the ultimate vertical displacement increased with increasing load angle. In addition, the load at which anchor slip began tended to increase with decreasing load angle. As a result, the vertical displacement at a particular tension load decreased as the load angle decreased. This trend was due to the influence of the shear load on the anchor slip load. The shear load, in forcing the anchor to bear against the wall of the hole, created a friction force between the shank of the anchor and the concrete. As a result, the applied tension load was transferred to the concrete by a combination of friction along the shank and friction at the wedge mechanism. Because the magnitude of frictional resistance along the shank was proportional to the shear load, it increased with decreasing load angle. Consequently, the fraction of tension load transferred at the wedge mechanism decreased as the load angle decreased, resulting in a delay in the onset of anchor slip.

For specimens with $l_d = 5.25$ in., the load angle did not significantly influence anchor deformation in the range of $\phi = 0$ to 60° . As shown in Figure 3.23(a), horizontal displacements were similar between different specimens except for Specimen 18 with $\phi = 60^\circ$, which had the smallest ultimate displacement and whose curve became nonlinear

at the smallest shear load. Horizontal displacements were less dependent on load angle than in specimens with $l_d = 4.0$ in. because the wedge mechanism was located farther from the concrete surface and thus was not as effective in contributing to concrete spalling. Table 3.4(b) shows that the spalling load for specimens with $l_d = 5.25$ in. was not as affected by load angle as in specimens with $l_d = 4.0$ in.

The effect of load angle on vertical displacement for specimens with $l_d = 5.25$ in. was only evaluated at $\phi = 45$ and 60° . As indicated in Figure 3.23(b), the load-displacement curves for specimens with $\phi = 45^\circ$ were nearly identical to that for the specimen with $\phi = 60^\circ$. Both curves for specimens with $\phi = 45^\circ$ showed a sudden increase in slope prior to failure. This phenomenon was also observed in specimens with $\phi = 45^\circ$ and $f_c \approx 6000$ psi in Figure 3.11(b).

In summary, increasing the load angle decreased the shear load at which spalling began and hence decreased the load at which the horizontal displacement curves became nonlinear. The influence of load angle on horizontal anchor displacement, however, decreased as the embedment depth increased from 4.0 to 5.25 in. Vertical anchor displacement was also affected by load angle at an embedment depth of 4.0 in. Decreasing the load angle from 90 to 60° resulted in a smaller vertical displacement at a particular tension load. Below a load angle of about 60° , the path of the vertical load-displacement curve was not significantly influenced.

3.3 Summary of Test Results

1. Anchor specimens with $\phi \leq 60^\circ$ failed in shear due to steel fracture. Steel fracture at the reduced section was the primary failure mode for specimens with $l_d = 4.0$ in. Increasing the embedment depth changed the failure mode to fracture at the shank for specimens with $\phi \leq 45^\circ$. At a particular load angle, the strength of anchors failing at the shank was generally larger than that of anchors failing at the reduced section.

2. Specimens with $\phi \geq 60^\circ$ failed in tension. One specimen with $\phi = 60^\circ$ experienced steel tensile failure at the threads, whereas specimens with $\phi = 70$ to 90° experienced cone-shaped tensile failure of the concrete.
3. Increasing the concrete compressive strength in the range of 4500 to 6000 psi did not significantly influence the strength and deformation behavior of anchors failing in shear.
4. Anchor behavior was variable for specimens subjected to pure shear loads. In addition, increasing the embedment depth from 4.0 to 5.25 in. for such anchors did not influence anchor behavior.
5. For specimens with $\phi = 45^\circ$, the ultimate shear load increased approximately linearly as the embedment depth increased from 3.5 to 6.0 in. At an embedment depth of 6.0 in., a limiting capacity was reached corresponding to steel failure at the shank due to pure shear stresses.
6. For specimens with $\phi = 60^\circ$, increasing the embedment depth from 4.0 to 6.25 in. resulted in an approximately linear increase in the ultimate shear load and a change in failure mode from shear to tension at an embedment depth between 5.25 and 6.25 in. The specimen with $l_d = 6.25$ in. experienced steel tensile failure at the threads and reached the limiting anchor tensile strength.
7. Increasing the embedment depth for specimens with $\phi = 45$ and 60° increased the load at which the horizontal and vertical components of the load-displacement curves became nonlinear and resulted in smaller horizontal and vertical displacements at a particular load.
8. For specimens with $l_d = 4.0$ and 5.25 in. that failed in shear, the ultimate shear load decreased as the load angle increased from 0 to 60° .
9. For specimens with $l_d = 4.0$ in. and $f_c \approx 4500$ psi which experienced cone-shaped concrete tensile failure, the ultimate tension load remained approximately constant as the load angle decreased from 90 to 70° .

10. The resultant capacity, P_u , increased approximately linearly as the embedment depth increased from 3.0 to 6.25 in. for specimens with $\phi = 0$ to 90° and $f_c \approx 4500$ to 6000 psi.

11. The resultant capacity was not significantly affected as the load angle increased from 0 to 90° for specimens with $l_d = 4.0$ in.

12. For specimens with $l_d = 4.0$ in. and $f_c \approx 4500$ psi, the load at which the horizontal and vertical load-displacement curves became nonlinear decreased as the load angle increased. The effect of load angle on horizontal displacement diminished as the embedment depth increased from 4.0 to 5.25 in.

Table 3.1 Test Results of Experimental Program

(a) Specimens With $f_c \approx 4500$ psi

Specimen	f_c (psi)	ϕ (deg.)	l_d (in.)	V_u (kips) ¹	T_u (kips) ²	Failure Mode ³
12	4350	0	4.00	15.4	0.0	SR
27	4670	0	4.00	34.0	0.0	SR
11	4350	0	5.25	31.0	0.0	SR
17	4920	0	5.25	29.8	0.0	SS
28	4670	22.5	4.00	25.7	10.8	SR
15	4350	45	4.00	17.8	18.0	SR
13	4350	45	5.25	27.3	27.8	SR
14	4350	45	5.25	33.9	34.2	SS
20	4920	60	4.00	15.4	26.9	SR
18	4920	60	5.25	22.4	39.1	SR
19	4920	60	6.25	26.3	46.0	TT
21	4670	70	4.00	9.6	26.5	TC
23	4670	80	4.00	4.2	23.9	TC
24	4670	90	4.00	0.0	24.9	TC

(b) Specimens With $f_c \approx 6000$ psi

Specimen	f_c (psi)	ϕ (deg.)	l_d (in.)	V_u (kips)	T_u (kips)	Failure Mode
31	5950	0	4.00	28.1	0.0	SR
33	5950	0	4.00	37.3	0.0	SS
32	5950	0	5.25	34.0	0.0	SS
2	5950	45	3.50	16.1	16.1	SR
8	6350	45	4.50	24.9	24.9	SR
9	6350	45	5.25	31.3	32.2	SS
1	5950	45	6.00	39.4	39.8	SS
3	5950	60	4.00	16.9	29.6	SR
10	6350	60	5.25	22.9	39.8	SR
4	5950	90	3.00	0.0	19.4	TC

¹ V_u = ultimate shear load applied to anchor

² T_u = ultimate tension load applied to anchor

³ SR: shear failure - steel fracture at reduced section

SS: shear failure - steel fracture at shank

TT: tension failure - steel tensile fracture at threads

TC: tension failure - cone-shaped concrete tensile failure

Table 3.2 Depth of Spalled Concrete for Specimens With $\phi = 45^\circ$

(a) Specimens With $f_c \approx 4500$ psi

Specimen	l_d (in.)	Maximum Depth of Spalling (in.)	Failure Mode
15	4.00	2.5	SR
13	5.25	1.5	SR
14	5.25	0.5	SS

(b) Specimens With $f_c \approx 6000$ psi

Specimen	l_d (in.)	Maximum Depth of Spalling (in.)	Failure Mode
2	3.50	2.0	SR
8	4.50	2.0	SR
9	5.25	1.0	SS
1	6.00	0.5	SS

Table 3.3 Effect of Load Angle on Ultimate Behavior

(a) Specimens With $l_d = 4.0$ in.

Specimen	f_c (psi)	ϕ (deg.)	V_u (kips)	T_u (kips)	P_u (kips) ¹	Failure Mode
27	4670	0	34.0	0.0	34.0	SR
31	5950	0	28.1	0.0	28.1	SR
33	5950	0	37.3	0.0	37.3	SS
28	4670	22.5	25.7	10.8	27.9	SR
15	4350	45	17.8	18.0	25.3	SR
20	4920	60	15.4	26.9	31.0	SR
3	5950	60	16.9	29.6	34.1	SR
21	4670	70	9.6	26.5	28.2	TC
23	4670	80	4.2	23.9	24.3	TC
24	4670	90	0.0	24.9	24.9	TC

(b) Specimens With $l_d = 5.25$ in.

Specimen	f_c (psi)	ϕ (deg.)	V_u (kips)	T_u (kips)	P_u (kips)	Failure Mode
11	4350	0	31.0	0.0	31.0	SR
17	4920	0	29.8	0.0	29.8	SS
32	5950	0	34.0	0.0	34.0	SS
13	4350	45	27.3	27.8	39.0	SR
14	4350	45	33.9	34.2	48.2	SS
9	6350	45	31.3	32.2	44.9	SS
18	4920	60	22.4	39.1	45.1	SR
10	6350	60	22.9	39.8	45.9	SR

(c) Specimens With $l_d = 6.0$ to 6.25 in.

Specimen	f_c (psi)	ϕ (deg.)	V_u (kips)	T_u (kips)	P_u (kips)	Failure Mode
1	5950	45	39.4	39.8	56.0	SS
19	4920	60	26.3	46.0	53.0	TT

$$^1 P_u = \sqrt{V_u^2 + T_u^2}$$

Table 3.4 Concrete Spalling Loads

(a) Specimens With $l_d = 4.0$ in.

Specimen	f_c (psi)	ϕ (deg.)	Spall Load V_{sp} (kips)
27	4670	0	14
28	4670	22.5	19
15	4350	45	14
20	4920	60	5
21	4670	70	5
23	4670	80	3

(b) Specimens With $l_d = 5.25$ in.

Specimen	f_c (psi)	ϕ (deg.)	Spall Load V_{sp} (kips)
11	4350	0	13
17	4920	0	15
13	4350	45	8
14	4350	45	16
18	4920	60	11

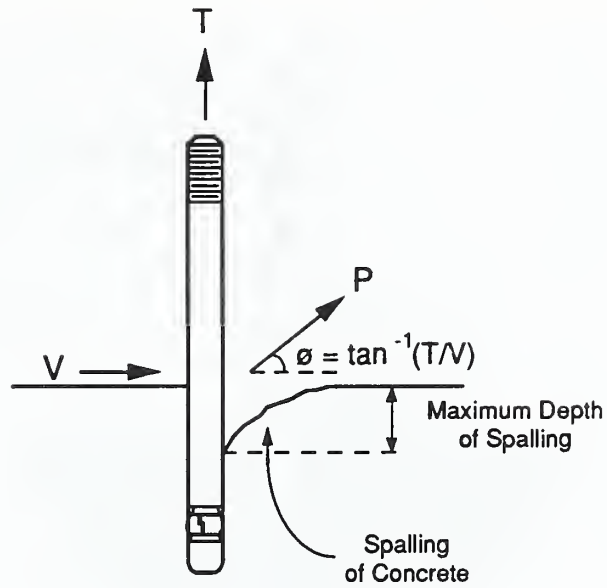


Figure 3.1 Applied Loading Condition

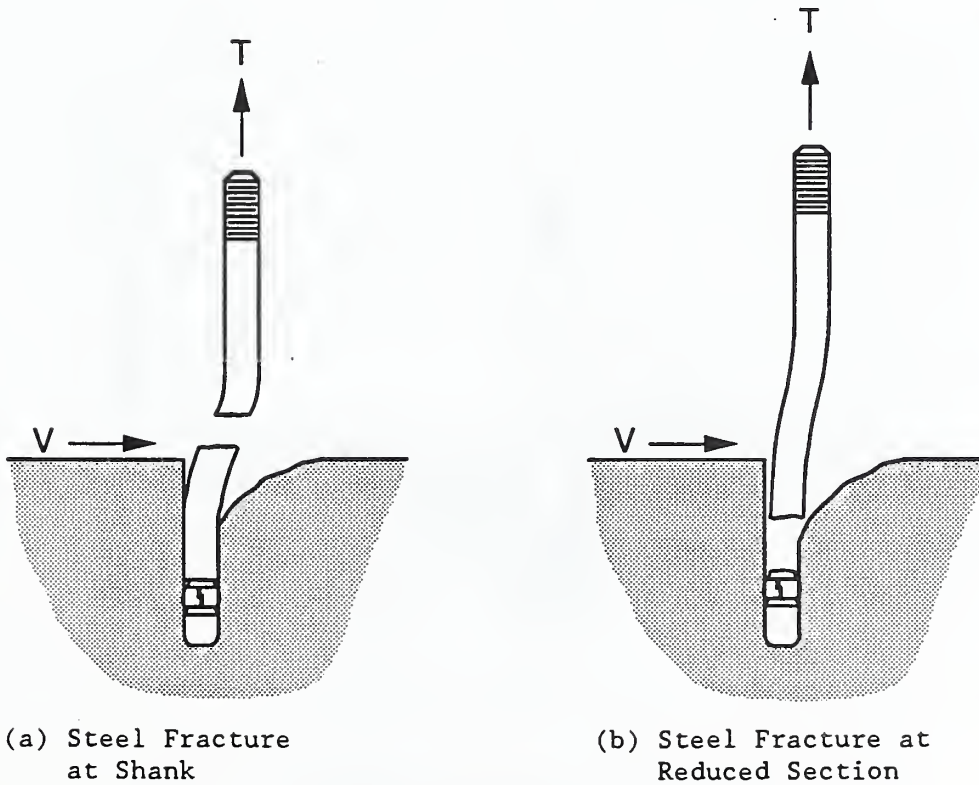
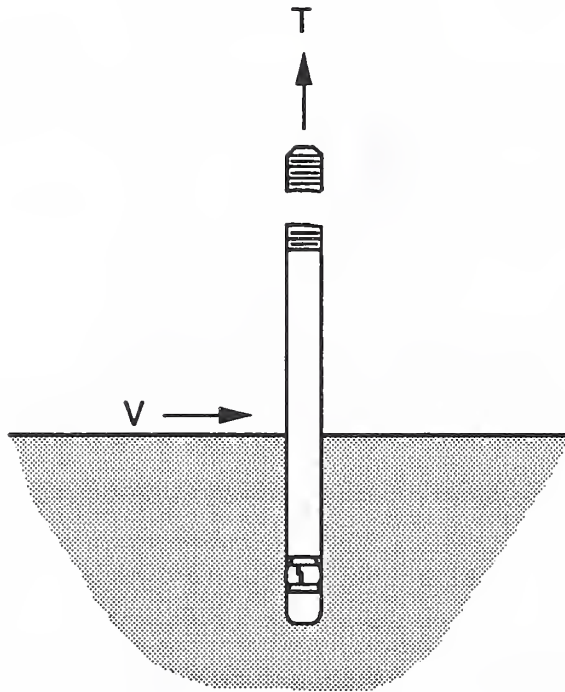
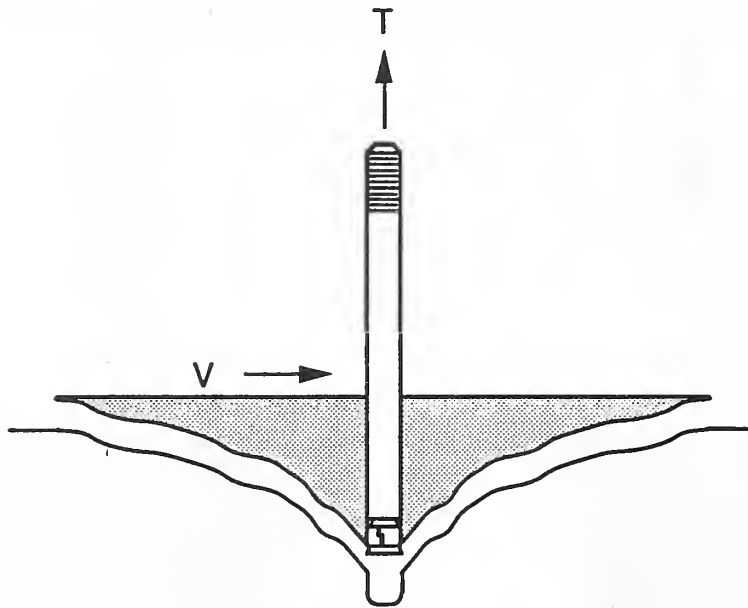


Figure 3.2 Types of Shear Failures

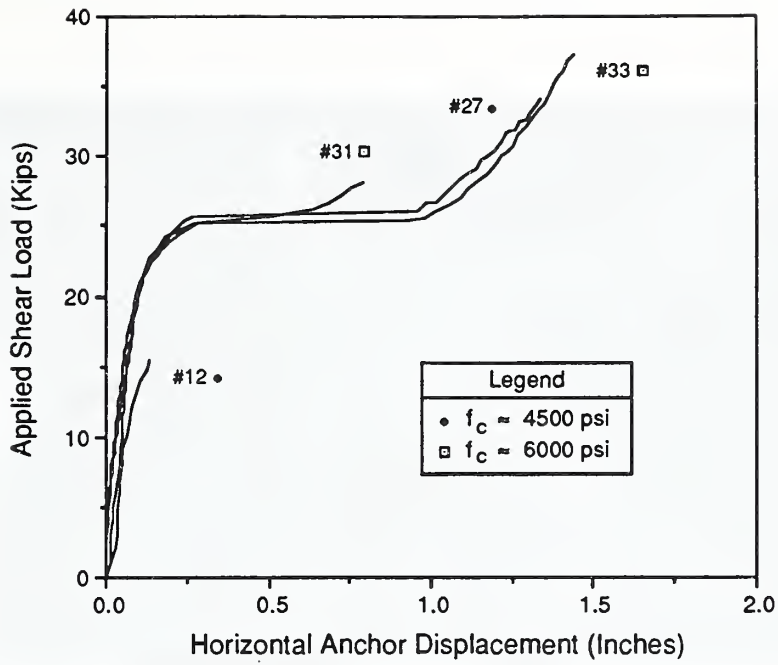


(a) Steel Fracture at Threads

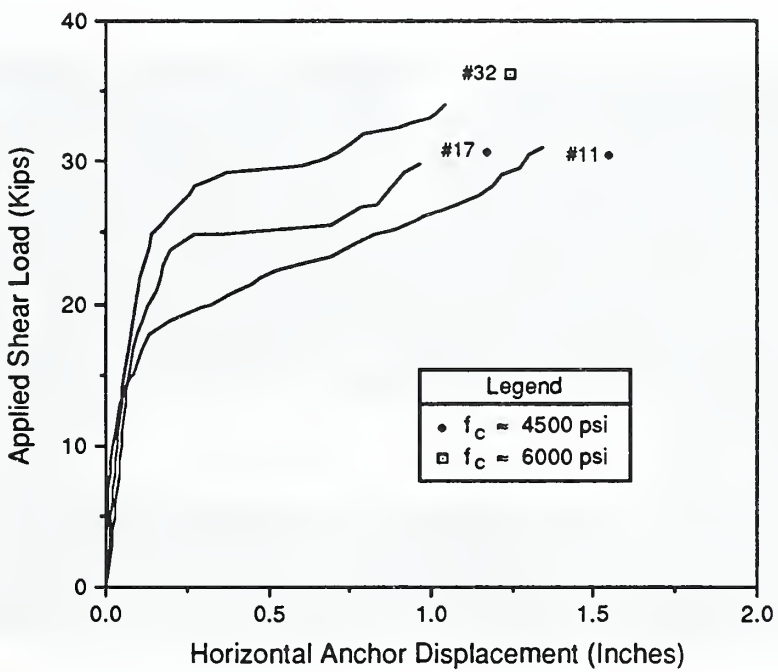


(b) Cone-Shaped Failure of Concrete

Figure 3.3 Types of Tension Failures

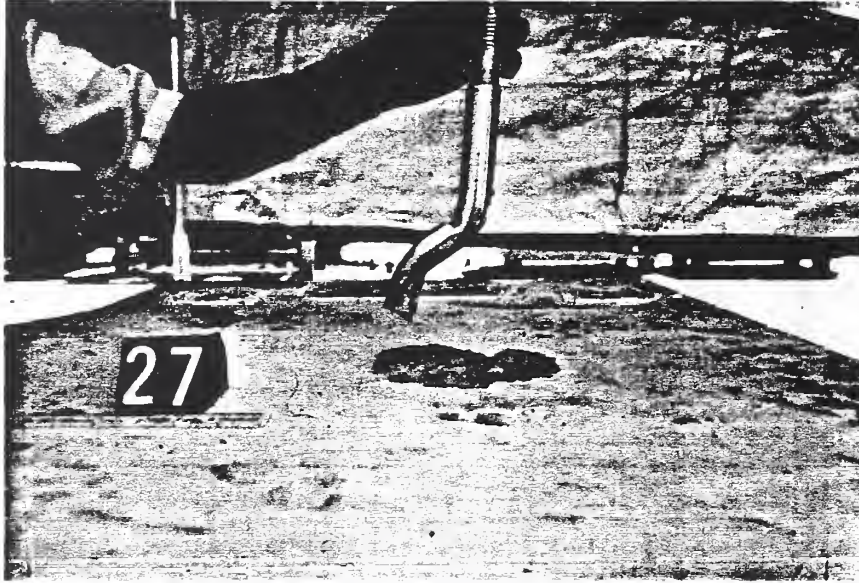


(a) Specimens With $l_d = 4.0$ in.



(b) Specimens With $l_d = 5.25$ in.

Figure 3.4 Load-Displacement Curves for Specimens With $\phi = 0^\circ$ and $l_d = 4.0$ and 5.25 in.

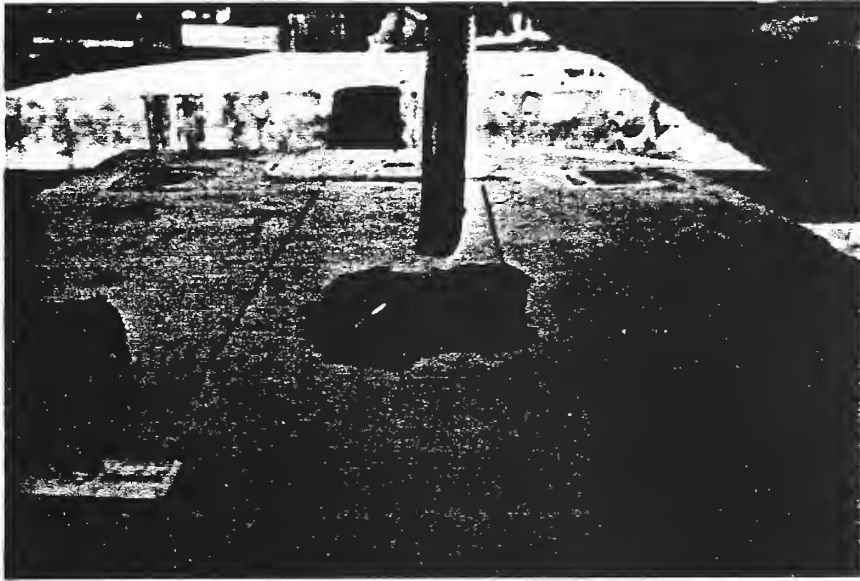


(a) Specimen 27 After Failure



(b) Failure Surface of Anchor

Figure 3.5 Anchor Fracture at Reduced Section of Specimen 27

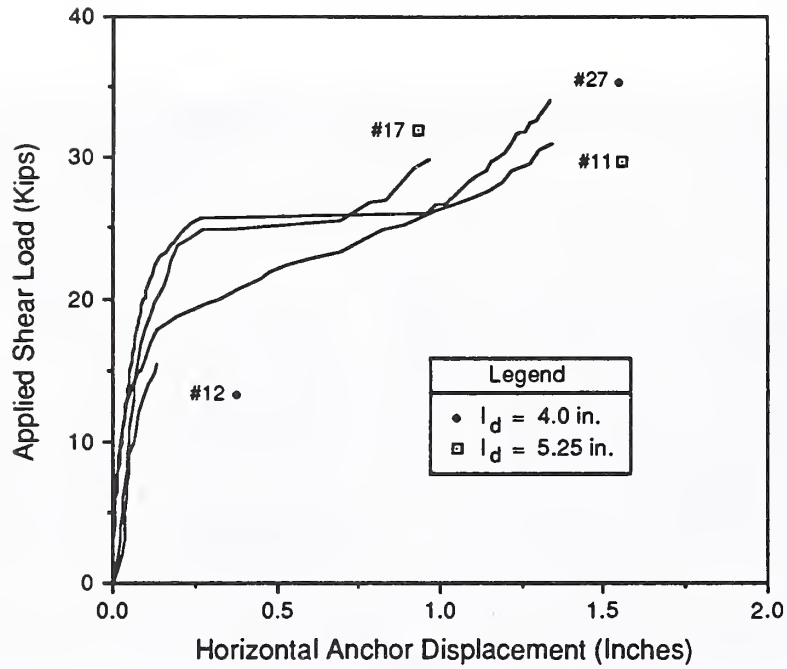


(a) Specimen 33 After Failure

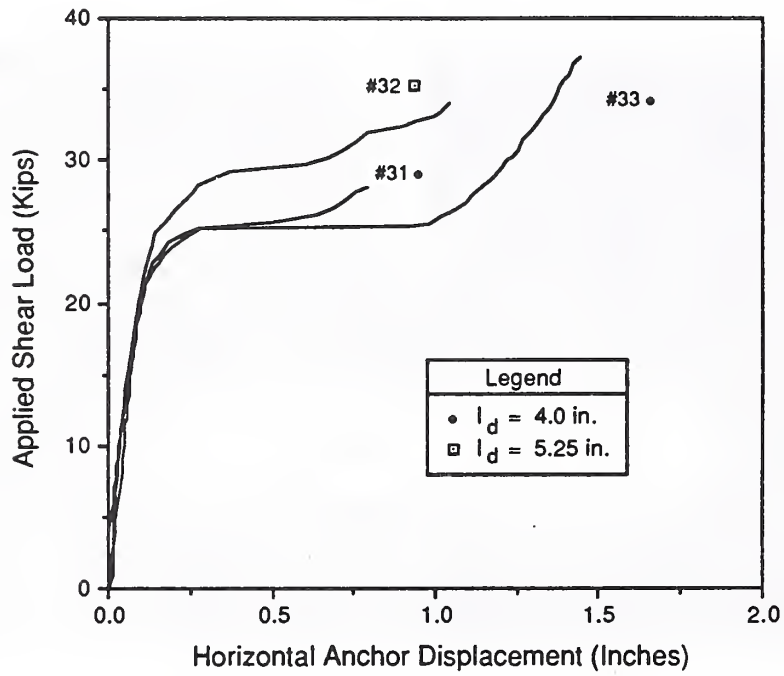


(b) Failure Surface of Anchor

Figure 3.6 Anchor Fracture at Shank of Specimen 33

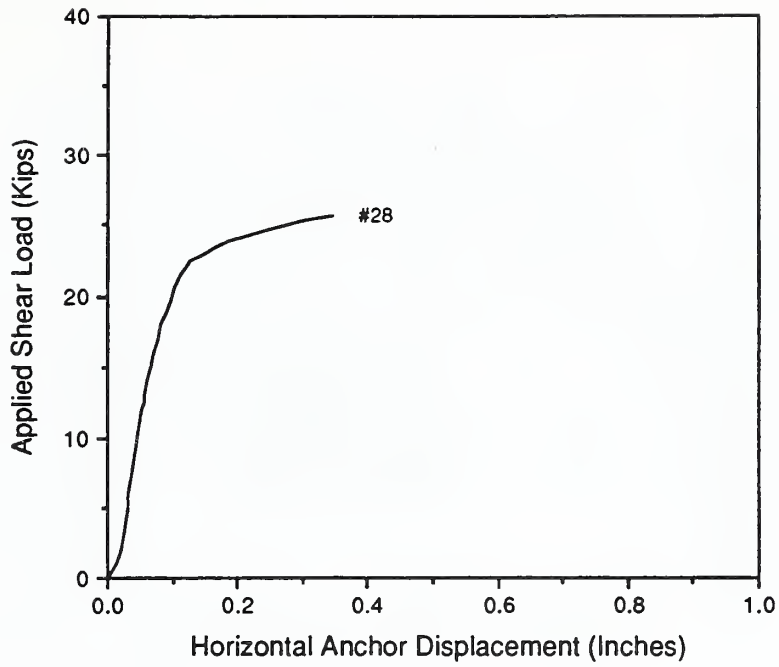


(a) Specimens With $f_c \approx 4500$ psi

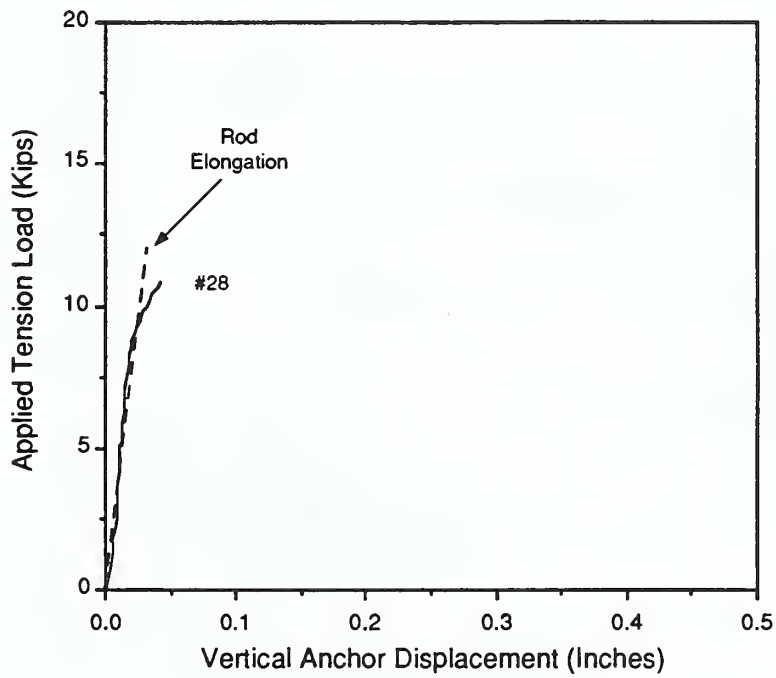


(b) Specimens With $f_c \approx 6000$ psi

Figure 3.7 Load-Displacement Curves for Specimens With $\phi = 0^\circ$ and $f_c \approx 4500$ and 6000 psi



(a) Horizontal Component



(b) Vertical Component

Figure 3.8 Load-Displacement Curve for Specimen With $\phi = 22.5^\circ$

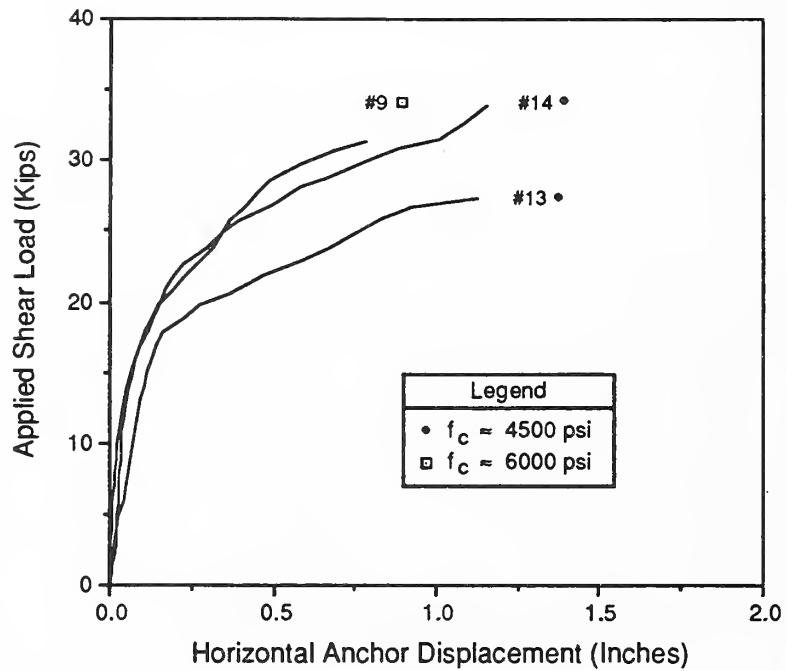


Figure 3.9 Horizontal Components of Load-Displacement Curves for Specimens With $\phi = 45^\circ$ and $l_d = 5.25$ in.

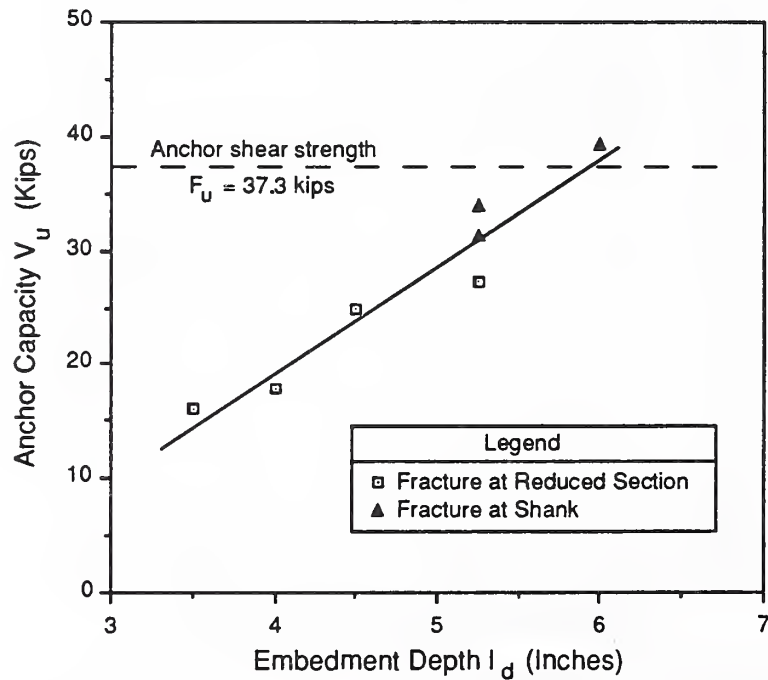
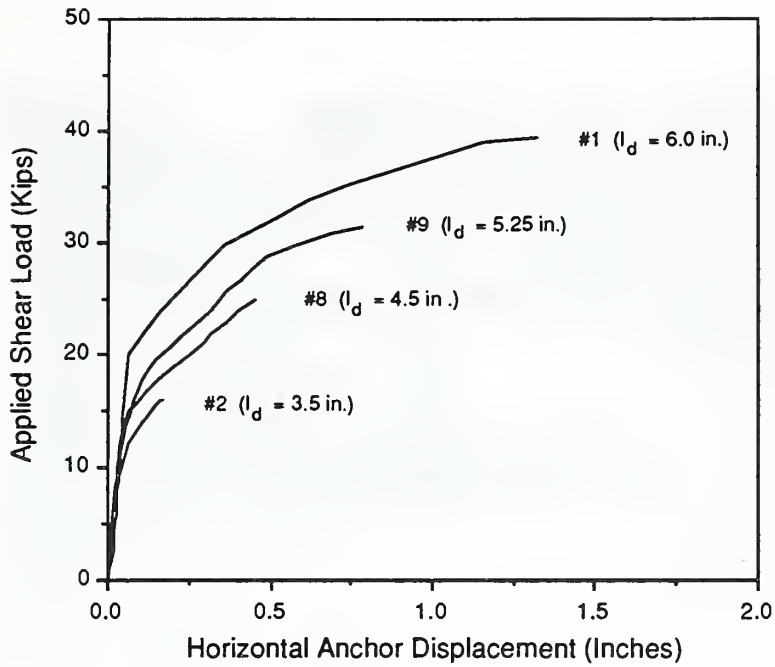
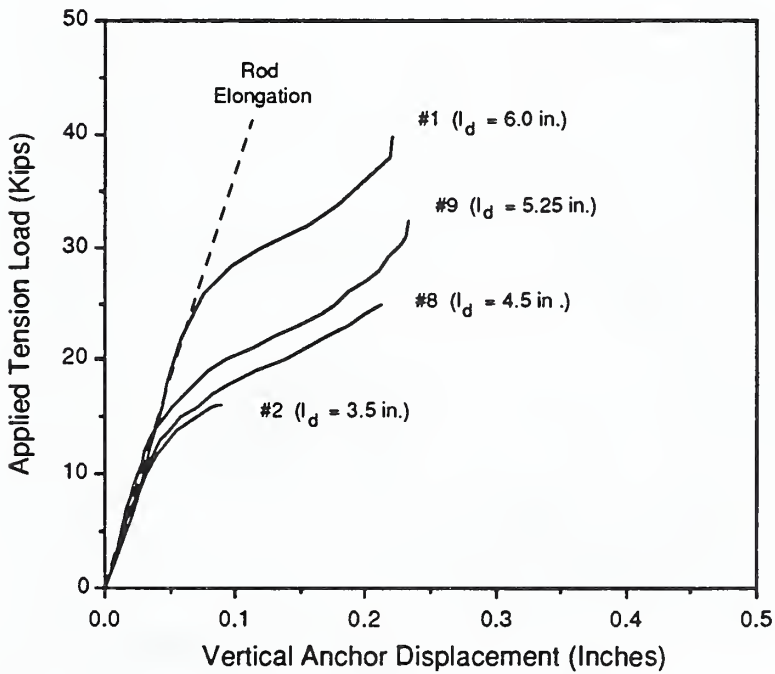


Figure 3.10 Anchor Capacity Versus Embedment Depth for Specimens With $\phi = 45^\circ$

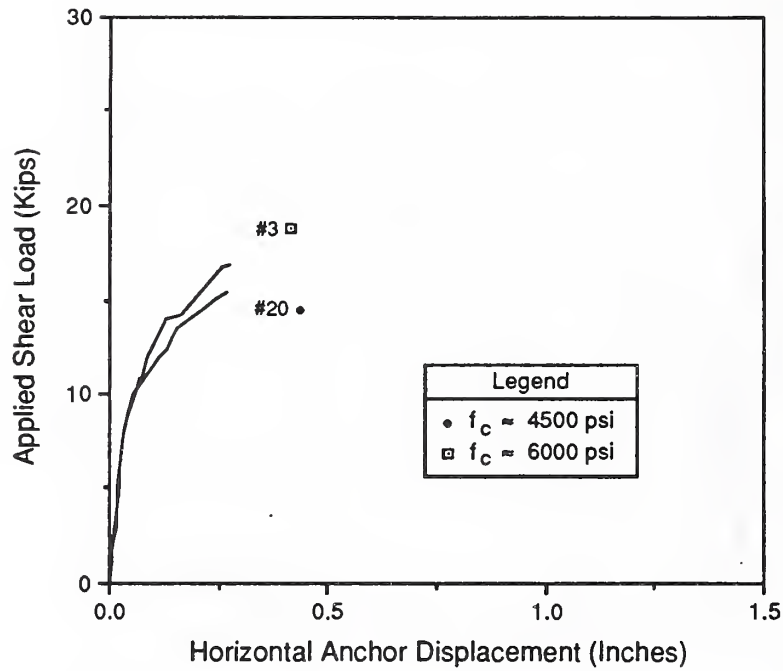


(a) Horizontal Components

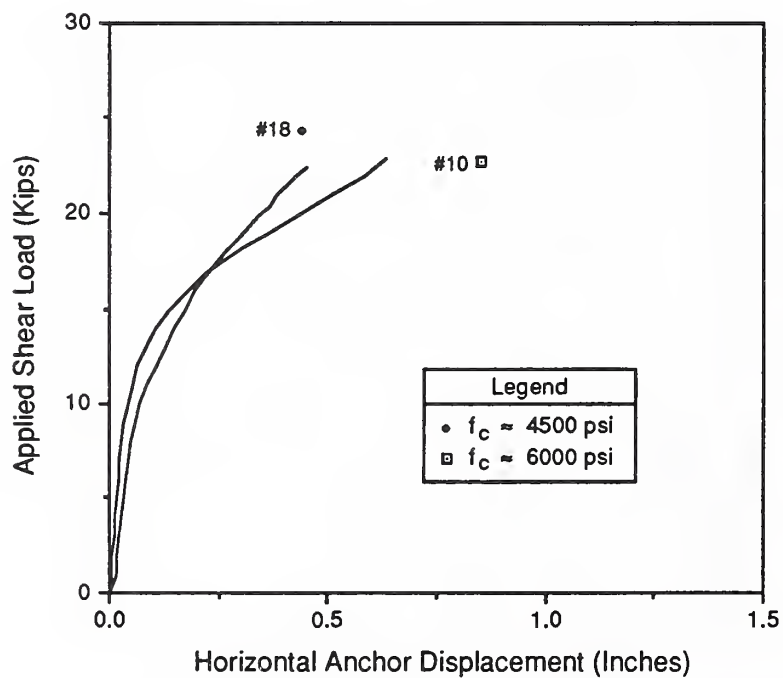


(b) Vertical Components

Figure 3.11 Load-Displacement Curves for Specimens With $\phi = 45^\circ$ and $f_c \approx 6000$ psi



(a) Specimens With $l_d = 4.0$ in.



(b) Specimens With $l_d = 5.25$ in.

Figure 3.12 Horizontal Components of Load-Displacement Curves for Specimens With $\phi = 60^\circ$ and $l_d = 4.0$ and 5.25 in.

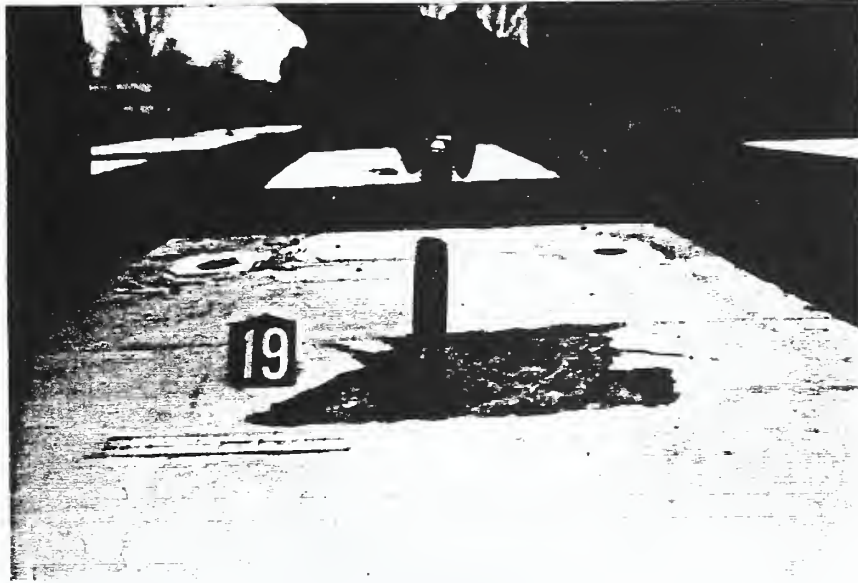


Figure 3.13 Anchor Tensile Failure at Threads of Specimen 19

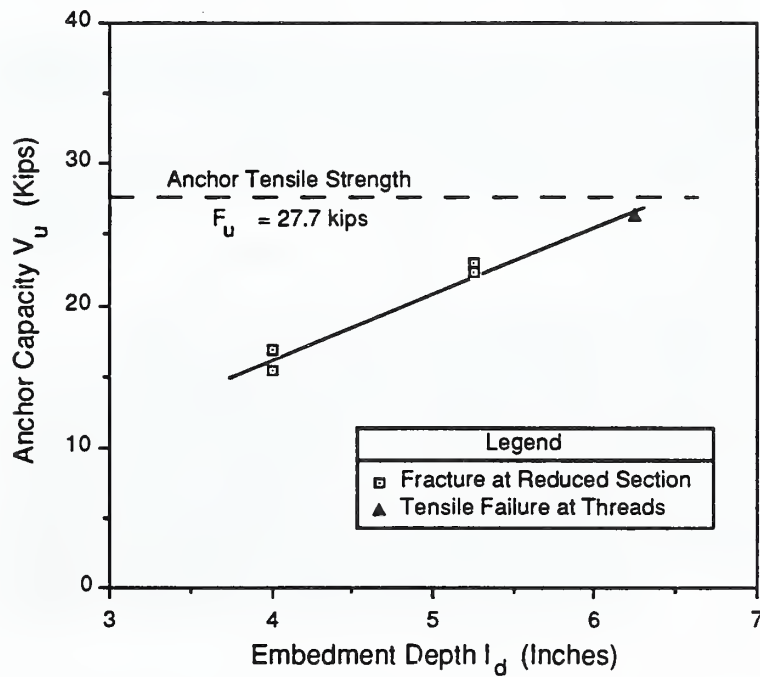
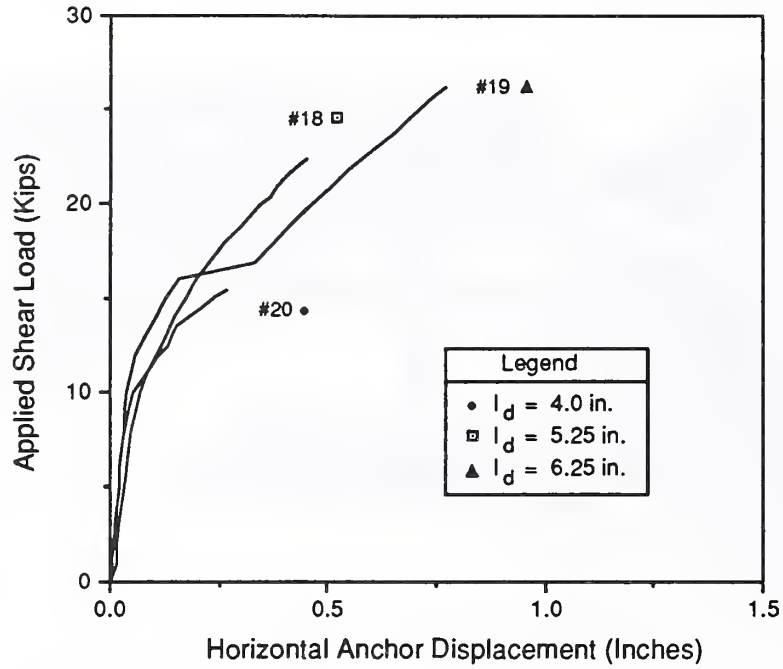
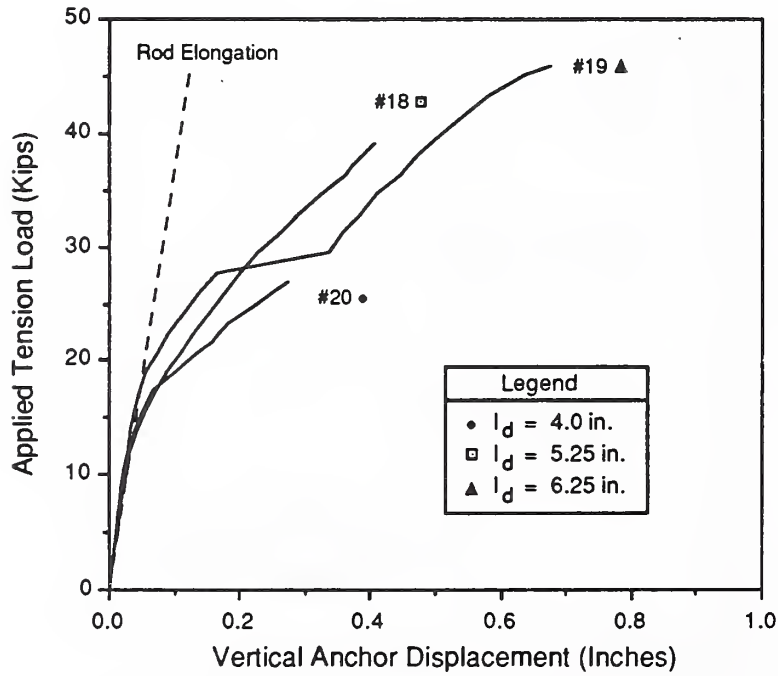


Figure 3.14 Anchor Capacity Versus Embedment Depth for Specimens With $\phi = 60^\circ$



(a) Horizontal Components



(b) Vertical Components

Figure 3.15 Load-Displacement Curves for Specimens With $\phi = 60^\circ$ and $f_c \approx 4500$ psi

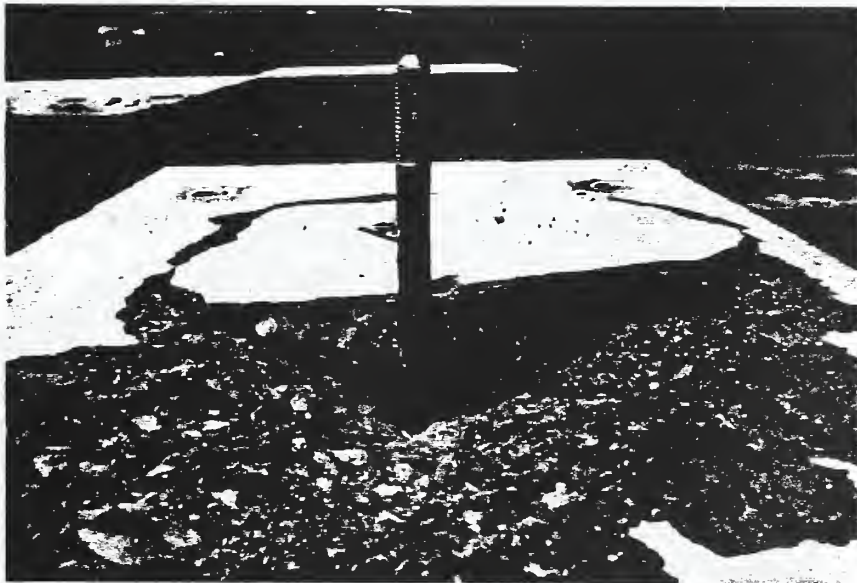
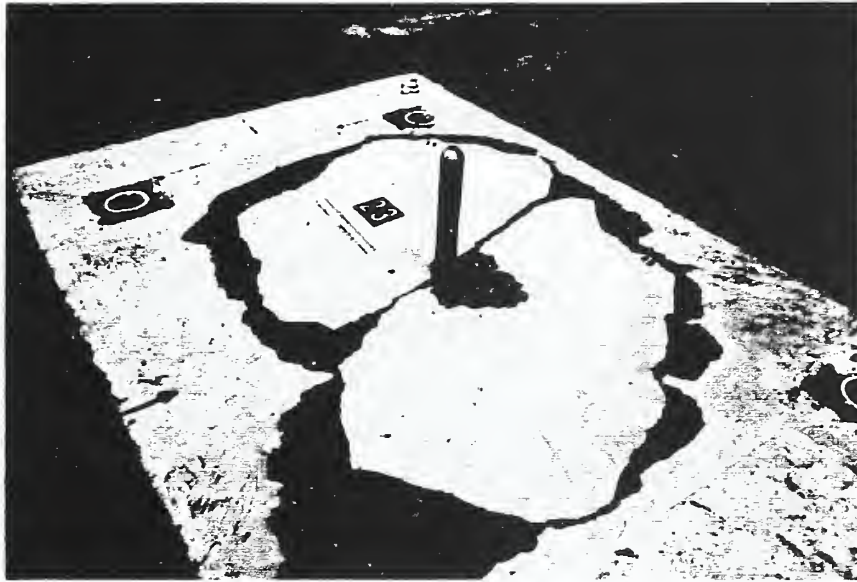
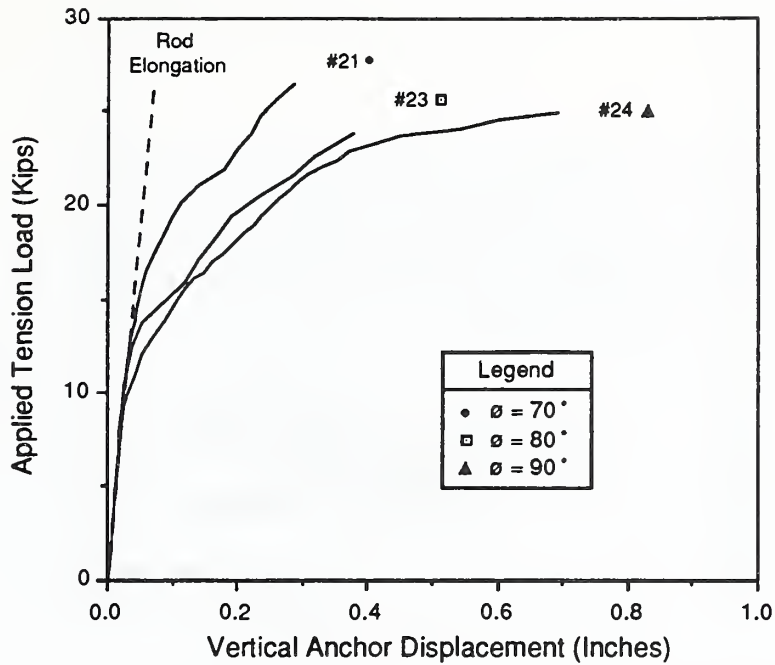


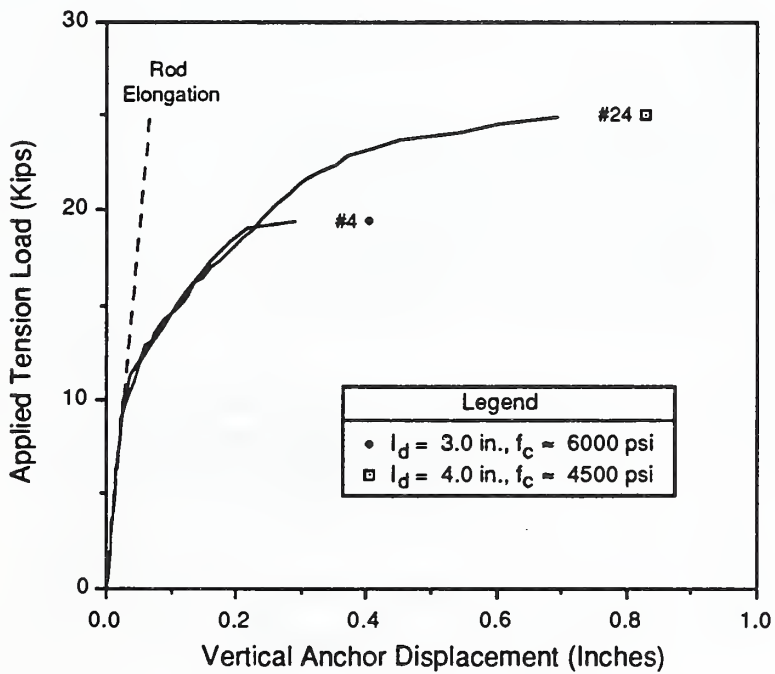
Figure 3.16 Broken Failure Cone of Specimen 23



Figure 3.17 Failure Cone of Specimen 4

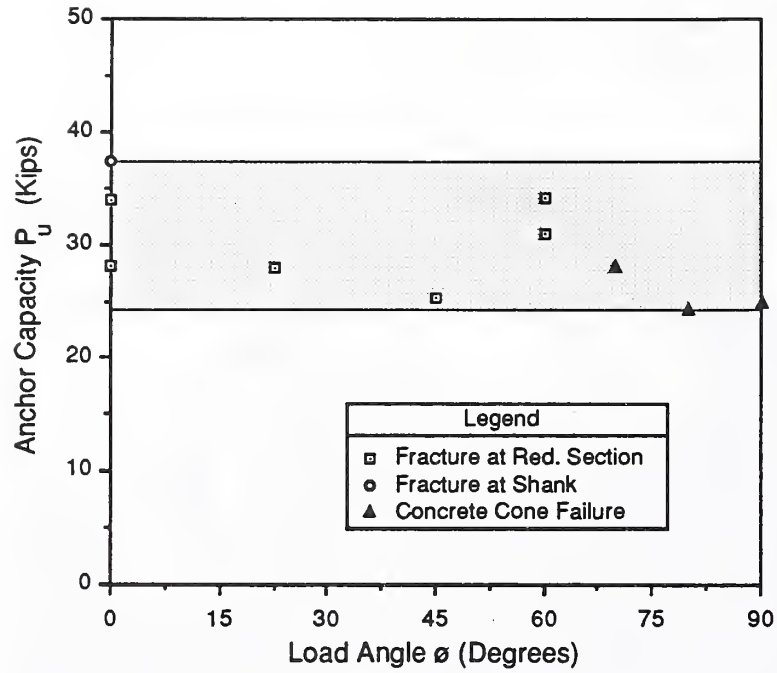


(a) Specimens With $f_c \approx 4500$ psi and $l_d = 4.0$ in.

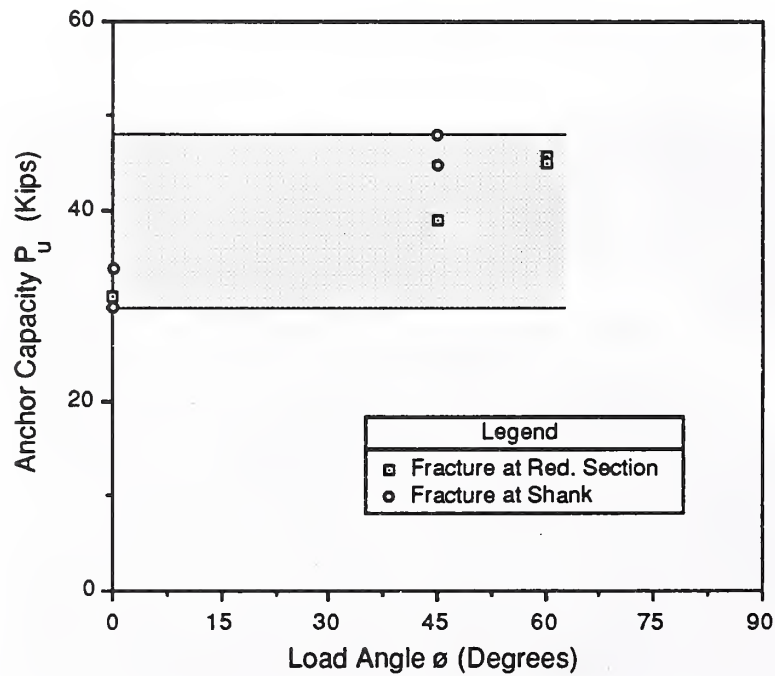


(b) Specimens With $\phi = 90^\circ$

Figure 3.18 Vertical Components of Load-Displacement Curves for Specimens With $\phi = 70$ to 90°

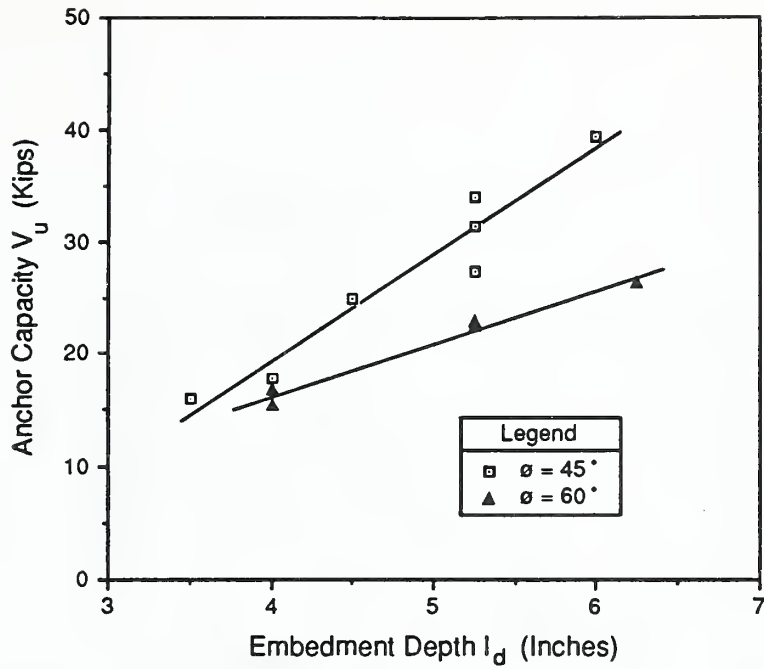


(a) Specimens With $l_d = 4.0$ in.

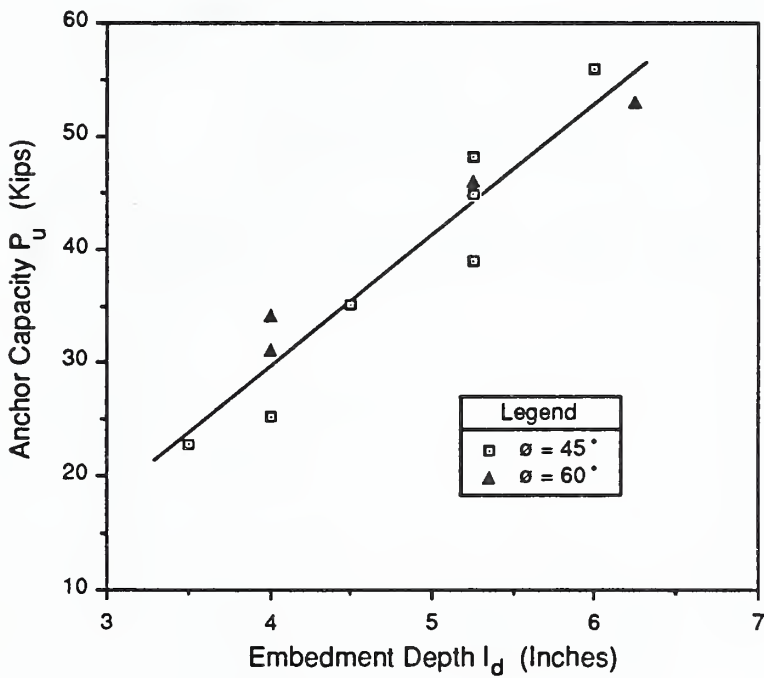


(b) Specimens With $l_d = 5.25$ in.

Figure 3.19 Anchor Capacity Versus Load Angle for Specimens With $l_d = 4.0$ and 5.25 in.



(a) Shear Capacity, V_u



(b) Resultant Capacity, P_u

Figure 3.20 Anchor Capacity Versus Embedment Depth for Specimens With $\phi = 45$ and 60°

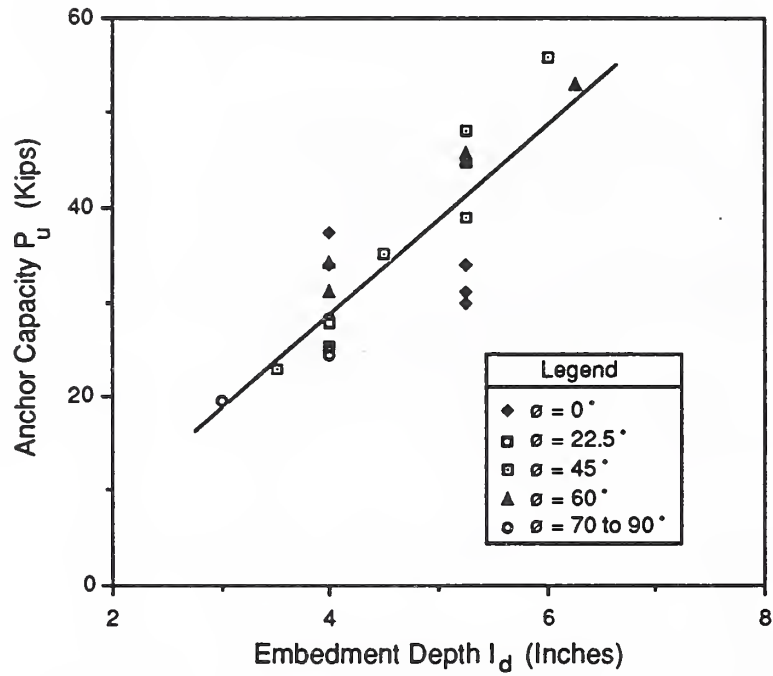
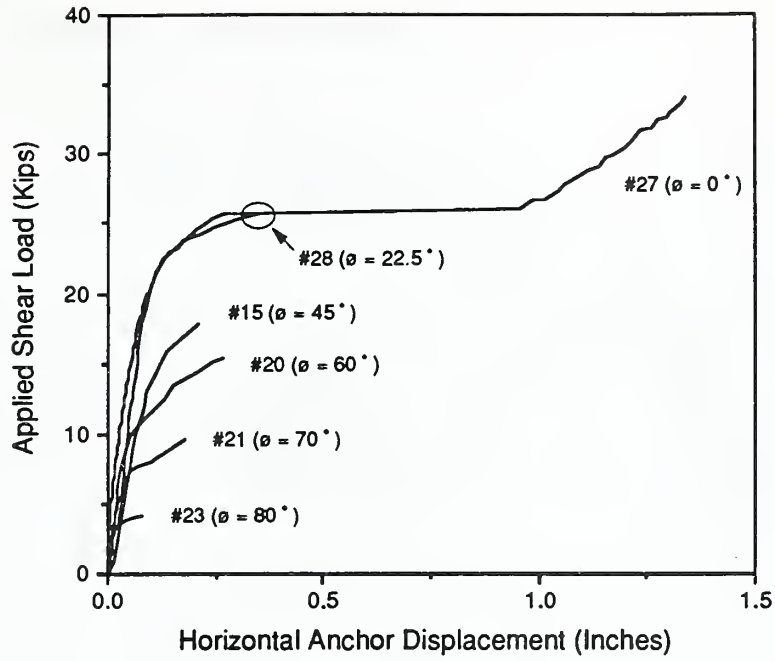
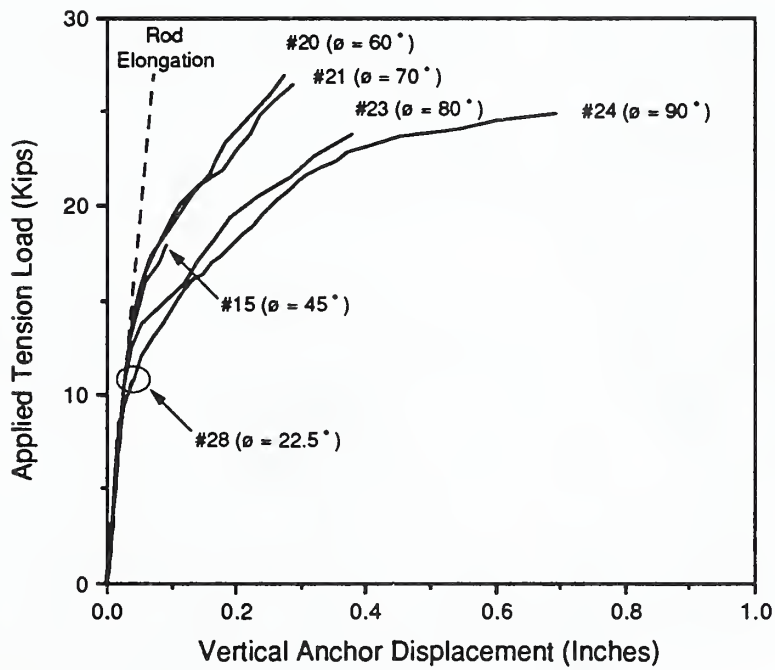


Figure 3.21 Anchor Capacity Versus Embedment Depth for Specimens With $\phi = 0$ to 90°

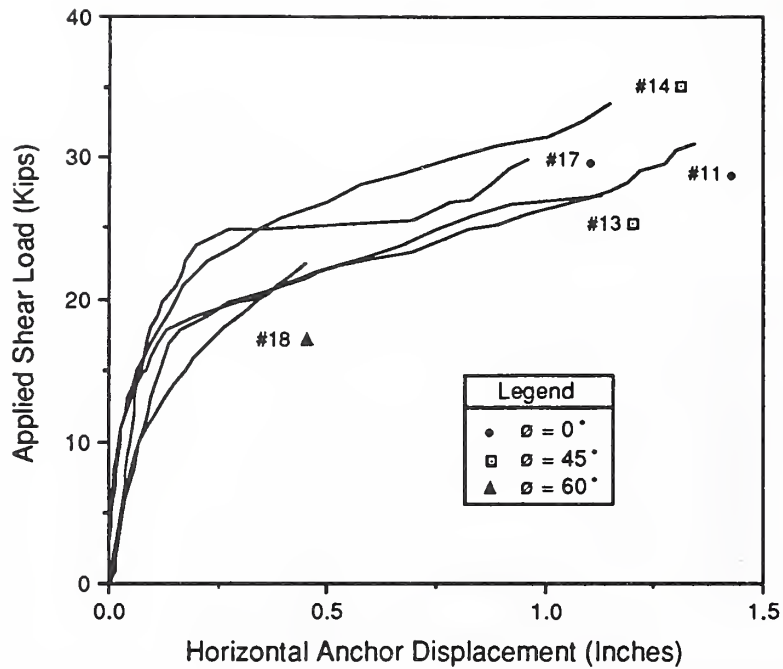


(a) Horizontal Components

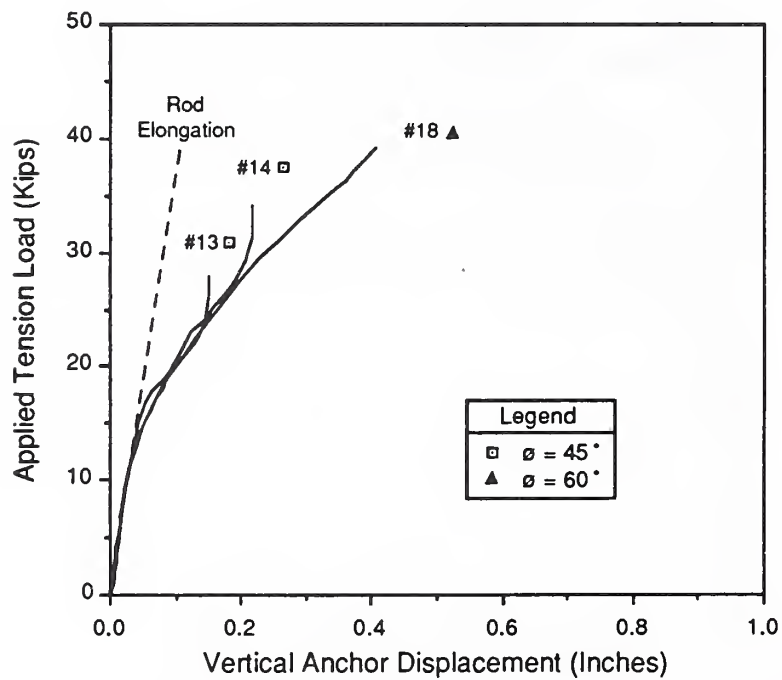


(b) Vertical Components

Figure 3.22 Load-Displacement Curves for Specimens With $l_d = 4.0$ in. and $f_c \approx 4500$ psi



(a) Horizontal Components



(b) Vertical Components

Figure 3.23 Load-Displacement Curves for Specimens With $l_d = 5.25$ in. and $f_c \approx 4500$ psi

4.0 DISCUSSION AND CONCLUSIONS

4.1 Discussion of Test Results

4.1.1 Deformation Behavior of Anchors

Deformation behavior of wedge-type anchors was examined in the horizontal and vertical directions, corresponding to the directions of the applied shear and tension loads, respectively. Anchor displacement was influenced by load angle and embedment depth. Concrete strength, which varied from 4500 to 6000 psi for specimens with $\phi \leq 60^\circ$, did not significantly affect anchor displacement.

Horizontal displacement behavior was similar in all anchor specimens. As shear load was applied, anchors initially experienced a slight nonlinear displacement due to movement of the anchor to the side of the hole. Horizontal displacement then increased approximately linearly as the shear load increased. This linear displacement corresponded to bearing of the anchor against the side of the hole. However, after concrete spalling occurred, the load-displacement curve became nonlinear as horizontal displacement increased significantly due to a loss of bearing support.

Embedment depth and load angle affected the shape of the horizontal displacement curve. Increasing the embedment depth increased the load at which spalling first occurred and thus delayed the onset of nonlinearity in the load-displacement curve. Consequently, the magnitude of horizontal displacement at a particular shear load decreased as the embedment depth increased. This trend was observed for specimens with $\phi = 45$ and 60° in which embedment depth varied over a relatively wide range. Increasing the load angle decreased the load at which the load-displacement curve became nonlinear because spalling began at a lower magnitude of shear load. This phenomenon was especially evident in specimens with $l_d = 4.0$ in.; horizontal displacement in specimens with $l_d = 5.25$ in. was not as dependent on

load angle because the wedge mechanism, being located farther away from the concrete surface, was less effective in contributing to spalling.

Vertical anchor displacement was similar to horizontal displacement in that it initially increased approximately linearly as the applied tension load increased. This linear displacement corresponded to elongation of the threaded rod and anchor bolt, although anchor elongation was so small as to be negligible. As the tension load increased, the vertical load-displacement curve eventually became nonlinear, indicating the beginning of anchor slip.

The presence of shear load influenced the tension load at which anchor slip began. For anchors subjected to pure tension ($\phi = 90^\circ$), the applied tension load was transferred by friction at the wedge mechanism. For such anchors, the anchor slip load was approximately 9 to 10 kips, regardless of embedment depth. This load corresponded to the magnitude of tension force applied to the wedge mechanism required to overcome initial seating of the wedge during installation. However, when shear load was applied, it created a friction force along the shank that combined with the friction force at the wedge to resist the applied tension load. As a result, the application of shear load increased the tension load at which anchor slip began, since less load was being transferred at the wedge mechanism. In fact, the magnitude of tension load at which slip began tended to increase with decreasing load angle for specimens with $l_d = 4.0$ in.

Except for anchors subjected to pure tension, embedment depth also influenced the anchor slip load. Increasing the embedment depth increased the load at which concrete spalling occurred. Because spalling diminished the friction force along the shank, it often resulted in the beginning of anchor slip. Consequently, increasing the embedment depth delayed the load at which anchor slip began, as observed in specimens with $\phi = 45$ and 60° .

4.1.2 Ultimate Behavior of Anchors

The effects of concrete strength and embedment depth on the ultimate behavior of wedge-type anchors depended on the failure mode. Anchors with $\phi \leq 60^\circ$ failed in shear due to steel fracture at either the reduced section or shank. The strength of such anchors was not significantly influenced by concrete strength; instead, it depended on the properties of the steel, the magnitude of bending stresses in the anchor, and the location of the fracture. The particular fracture location depended mainly on embedment depth. Anchors with relatively shallow embedment depths fractured at the reduced section due to the section's proximity to the concrete surface. As the embedment depth increased, however, the reduced section became located far enough away from the concrete surface so that steel fracture occurred along the shank. The strength of anchors failing at the shank was generally larger than that of anchors failing at the reduced section.

The strength of anchors experiencing steel fracture also depended on the magnitude of bending stresses in the anchor. Concrete spalling increased the bending moment induced in the anchor due to the eccentricity of the shear load. The resulting bending stresses combined with shear and tension stresses to cause fracture of the anchor. The magnitude of bending stresses lessened as the embedment depth increased because the depth of spalling decreased. Consequently, anchor strength increased with increasing embedment depth. For specimens with $\phi = 45^\circ$ and 60° , in fact, anchor capacity increased approximately linearly with embedment depth.

A limiting anchor capacity was reached when the embedment depth was sufficiently large so that bending stresses were negligible. This limit corresponded to steel shear failure at the shank and depended only on steel properties and anchor geometry. One specimen with $\phi = 45^\circ$ reached the limiting capacity at an embedment depth of 6 in. (In addition, one specimen with $\phi = 0^\circ$ reached this limit at an embedment depth of only 4 in.; however, the average strength of specimens with $l_d = 4.0$ in. at

$\phi = 0^\circ$ was significantly less than the limiting capacity.) Thus, it is reasonable to expect that anchors with $\phi < 45^\circ$ would reach a limiting strength at an embedment depth of approximately 6 in., since it was observed that differences in load-displacement behavior between specimens with different load angles tended to diminish as the embedment depth increased.

Anchors with $\phi = 60^\circ$ experienced both shear and tension failures. Increasing the embedment depth increased anchor strength and resulted in a change in failure mode from steel fracture at the reduced section to steel tensile failure at the threads at an embedment depth between 5.25 and 6.25 in. Steel tensile failure represented the limiting tensile strength of the anchor and was similar to the limiting shear strength in that it was easy to predict and depended only on steel properties and anchor geometry. Both the limiting shear and tensile capacities occurred at an embedment depth of approximately 6 in., regardless of the type of steel fracture.

Anchors with $\phi = 70$ to 90° failed in tension and experienced cone-shaped tensile failure of the concrete. The effects of concrete strength and embedment depth on anchor behavior were not isolated; however, the strength is expected to increase with increasing concrete strength and embedment depth. Because such a failure depends on the tensile strength of the concrete, an inherently variable parameter, the capacity is difficult to predict. However, in Reference 9, an empirical equation (Equation (3)) was developed to predict the strength of anchors subjected to pure tension experiencing cone-shaped concrete failure. Based on this equation, the capacity is proportional to $l_d^{1.54}$, in contrast to anchors experiencing steel failure in which the capacity was observed to increase approximately linearly with embedment depth.

Cone-shaped concrete failure was only investigated for anchors with embedment depths up to 4.0 in. Increasing the embedment depth beyond this value would increase the strength, but eventually a limit would be reached. Because the volume of the concrete cone increases with

embedment depth, this volume would be limited by the size of the member in which the anchor is embedded or by cones of surrounding anchors. Alternatively, some other mode of failure such as steel tensile fracture or anchor pullout would control for large embedment depths.

Although the load angle influenced the failure mode, it was not found to significantly affect anchor strength. The resultant strength increased linearly with increasing embedment depth, approximately independent of load angle. However, this trend was observed for specimens with concrete strengths in the range of 4500 to 6000 psi. For specimens with concrete strengths outside this range, it is possible that the load angle would affect anchor capacity.

To examine the effect of load angle on the strength of anchor specimens with a wider range of concrete strength, the results of a testing program conducted by Teledyne[5] are presented in Figure 4.1 in the form of interaction diagrams. The Teledyne program included a large number of combined shear and tension tests on different types of post-installed anchors in uncracked concrete, of which the results for wedge-type anchors are shown in Figure 4.1. Anchors were tested at load angles of 0, 22.5, 45, 67.5, and 90°. The concrete strength exceeded 3000 psi; no further specification was provided.

Figure 4.1(a) presents test results for specimens with anchor diameters of 1 in. and embedment depths of 4.5 in. Figure 4.1(b) presents test results for anchors with diameters ranging from 1/2 to 1-1/4 in. and embedment depths ranging from 1.25 to 4.5 in. Figure 4.1(a) also includes results for specimens of this NIST test program having $l_d = 4.0$ in. and $f_c \approx 4500$ to 6000 psi. The terms V_o and T_o in the diagrams represent the strength of anchors subjected to pure shear and pure tension loads, respectively.

Figure 4.1(a) shows that the test results of this program compared well with those of Reference 5. The data for Reference 5 cluster into three groups corresponding to the three load angles tested between 0 and

90°. The group of data points closest to the abscissa corresponds to anchors with $\phi = 22.5^\circ$, the next group consists of anchors with $\phi = 45^\circ$, and the group closest to the ordinate is that of anchors with $\phi = 67.5^\circ$.

The interaction diagrams show the resultant capacity to be somewhat dependent on the load angle. The resultant load capacity is defined as $P_u = \sqrt{V_u^2 + T_u^2}$, so that it would plot as a quarter circle with a radius of 1.0 on the interaction diagram if it was constant for all values of load angle. Test values for anchors with small load angles tend to lie inside the circle, whereas test values for anchors with larger load angles tend to lie on or outside the circle. This trend is illustrated in Figure 4.1(a), in which test data for anchors with $\phi = 22.5$ and 45° are located almost completely inside the circle and data for anchors with $\phi > 45^\circ$ are located mostly outside the circle.

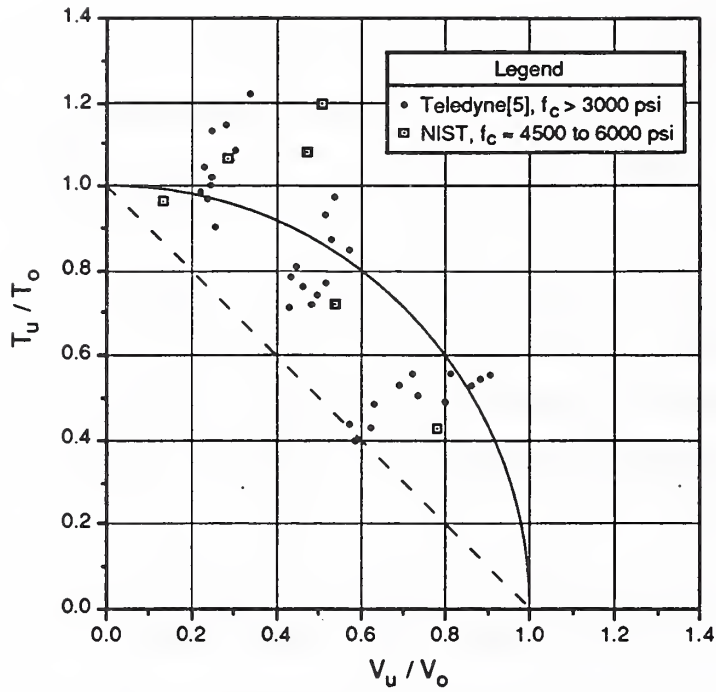
The diagrams indicate a large amount of scatter in the data. Because of this scatter, fitting a curve to the data is difficult. However, the straight dashed line, while not approximating the data, indicates a reasonable lower bound for anchor capacity. However, it does not take advantage of the fact that the data tend to become located farther from the origin as the load angle increases. Reference 7, which analyzed a comprehensive set of expansion anchor data, recognized this trend and recommended the use of two curves (circular and bilinear) to approximate combined shear and tension test data. Meinheit and Heidbrink[6], who also analyzed expansion anchor data, recommended the use of a trilinear curve as an approximation. ACI 349, Appendix B[10] bases design of post-installed anchors on a straight line approach.

In summary, the effect of such parameters as embedment depth and concrete strength on the ultimate behavior of wedge-type anchors depended on the magnitude of the load angle. For load angles up to 60° , failure was due to fracture of the anchor. The strength of such anchors was primarily dependent on embedment depth. For load angles between 70 and 90° , in which cone-shaped failure of the concrete occurred, the strength depended on both concrete strength and embedment depth.

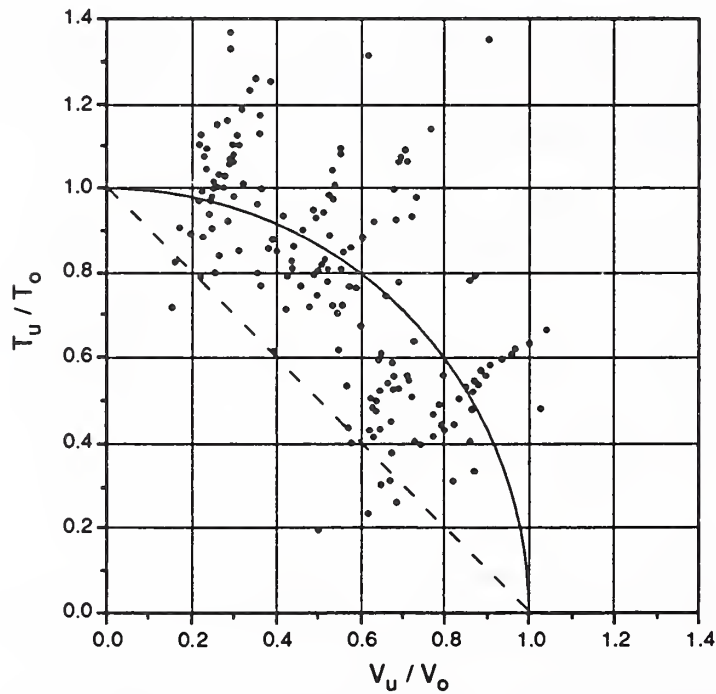
4.2 Conclusions

Based on the results of this experimental program, the following conclusions are made regarding 1 in. diameter wedge-type anchors embedded in uncracked concrete with large edge distance:

1. The mode of failure changes from shear to tension at a load angle of approximately 60° . Anchor capacity is limited by steel strength for anchors tested at load angles between 0 and 60° , whereas anchor capacity is limited by concrete strength for anchors tested at load angles between 70 and 90° .
2. The ultimate behavior of anchors failing in shear is primarily dependent on embedment depth. For such anchors, increasing the embedment depth changes the mode of failure from steel fracture at the reduced cross section to fracture at the shank.
3. The limiting anchor capacity occurs at an embedment depth of approximately 6 in. when steel failure controls, regardless of whether the failure mode is shear or tension.
4. Anchor deformation is influenced by both load angle and embedment depth.



(a) Anchors With Diameters of 1 in. and $l_d = 4.0$ to 4.5 in.



(b) Anchors With Diameters of 1/2 to 1-1/4 in. and $l_d = 1.25$ to 4.5 in. (from Teledyne[5])

Figure 4.1 Interaction Diagrams for Wedge-Type Anchors

REFERENCES

1. Phan, L.T., Lew, H.S., and Johnson, M.K., "Literature Review of Strengthening Methodologies of Existing Structures," NBSIR 88-3796, National Bureau of Standards, June 1988, 114 pp.
2. Johnson, M.K., Lew, H.S., and Phan, L.T., "Literature Review of Post-Installed Anchorage in Concrete," NBSIR 88-3797, National Bureau of Standards, June 1988, 59 pp.
3. Cannon, R.W., Burdette, E.G., and Funk, R.R., "Anchorage to Concrete," Report No. CEB 75-32, Tennessee Valley Authority, Knoxville, TN, 1975.
4. Lindquist, M.R., "Final Report, USNRC Anchor Bolt Study, Data Survey and Dynamic Testing," NUREG/CR-2999, Report No. HEDL-MISC-7246, Hanford Engineering Development Laboratory, December 1982.
5. "Summary Report, Generic Response to USNRC I&E Bulletin Number 79-02, Base Plate/Concrete Expansion Anchor Bolts," Technical Report 3501-1, Revision 1, Teledyne Engineering Services, August 1979.
6. Meinheit, D.F. and Heidbrink, F.D., "Behavior of Drilled-In Expansion Anchors," Concrete International, Design and Construction, Vol. 7, No. 4, April 1985, pp. 62-66.
7. "Seismic Verification of Nuclear Plant Equipment Anchorage, Vol. 1: Development of Anchorage Guidelines," NP-5228, Volume 1, Research Project 1707-16, URS Corporation/John A. Blume & Associates, Engineers, May 1987.
8. Manual of Steel Construction - Load & Resistance Factor Design, First Edition, American Institute of Steel Construction, Inc., 1986.
9. Eligehausen, R., "Anchorage to Concrete by Metallic Expansion Anchors," Anchorage to Concrete, SP 103-10, American Concrete Institute, Detroit, 1987, pp. 181-201.
10. ACI Committee 349, "Code Requirements for Nuclear Safety Related Concrete Structures," Appendix B - Steel Embedments, American Concrete Institute, Detroit, 1980.

1. PUBLICATION OR REPORT NUMBER NISTIR 90-4274
2. PERFORMING ORGANIZATION REPORT NUMBER
3. PUBLICATION DATE March 1990

BIBLIOGRAPHIC DATA SHEET

4. TITLE AND SUBTITLE
Experimental Study of Post-Installed Anchors Under Combined Shear and Tension Loading

5. AUTHOR(S)
Mark K. Johnson, H. S. Lew

6. PERFORMING ORGANIZATION (IF JOINT OR OTHER THAN NIST, SEE INSTRUCTIONS)
U.S. DEPARTMENT OF COMMERCE
NATIONAL INSTITUTE OF STANDARDS AND TECHNOLOGY
GAITHERSBURG, MD 20899

7. CONTRACT/GRANT NUMBER
8. TYPE OF REPORT AND PERIOD COVERED

9. SPONSORING ORGANIZATION NAME AND COMPLETE ADDRESS (STREET, CITY, STATE, ZIP)

10. SUPPLEMENTARY NOTES

DOCUMENT DESCRIBES A COMPUTER PROGRAM; SF-185, FIPS SOFTWARE SUMMARY, IS ATTACHED.

11. ABSTRACT (A 200-WORD OR LESS FACTUAL SUMMARY OF MOST SIGNIFICANT INFORMATION. IF DOCUMENT INCLUDES A SIGNIFICANT BIBLIOGRAPHY OR LITERATURE SURVEY, MENTION IT HERE.)
The behavior of post-installed anchors subjected to static combined shear and tension loads was studied experimentally. Twenty-four 1 in. diameter wedge-type expansion anchors were tested in uncracked concrete. Anchors were not preloaded and were located sufficiently far from the edge of the concrete specimens. Test variables included the angle of inclination of applied load (measured with respect to a horizontal plane), anchor embedment depth, and concrete compressive strength. Shear failures occurred for specimens tested at load angles between 0 and 60° and tension failures were observed for specimens tested at load angles between 60 and 90°. There were two types of shear failures: steel fracture near the bottom of the anchor at the tapered section for anchors with shallow embedment depths and steel fracture along the shank for more deeply-embedded anchors. Two types of tension failures occurred: steel tensile failure at the threads and cone-shaped tensile failure of the concrete. For specimens failing in shear, anchor capacity depended mainly on embedment depth. A limiting capacity was reached at an embedment depth of approximately 6 in. when steel failure controlled. Anchor deformation was influenced by both load angle and embedment depth.

12. KEY WORDS (6 TO 12 ENTRIES; ALPHABETICAL ORDER; CAPITALIZE ONLY PROPER NAMES; AND SEPARATE KEY WORDS BY SEMICOLONS)
anchors; combined loading; concrete; embedment depth; expansion anchors; post-installed anchors; shear; tension

13. AVAILABILITY

<input checked="" type="checkbox"/>	UNLIMITED
<input type="checkbox"/>	FOR OFFICIAL DISTRIBUTION. DO NOT RELEASE TO NATIONAL TECHNICAL INFORMATION SERVICE (NTIS).
<input type="checkbox"/>	ORDER FROM SUPERINTENDENT OF DOCUMENTS, U.S. GOVERNMENT PRINTING OFFICE, WASHINGTON, DC 20402.
<input checked="" type="checkbox"/>	ORDER FROM NATIONAL TECHNICAL INFORMATION SERVICE (NTIS) SPRINGFIELD, VA 22161

14. NUMBER OF PRINTED PAGES
81

15. PRICE
A05

